1

The dual function monoclonal antibodies VIR-7831 and VIR-7832 demonstrate potent in vitro and in vivo activity against SARS-CoV-2

Andrea L. Cathcart[1], Colin Havenar-Daughton[1], Florian A. Lempp[1], Daphne Ma[1], Michael A. Schmid[2], Maria L. Agostini[1], Barbara Guarino[2], Julia Di iulio[1], Laura E. Rosen[1], Heather Tucker[1], Joshua Dillen[1], Sambhavi Subramanian[1], Barbara Sloan[1], Siro Bianchi[2], Dora Pinto[2], Christian Saliba[2], Jason A Wojcechowskyj[1], Julia Noack[1], Jiayi Zhou[1], Hannah Kaiser[1], Arthur Chase[1], Martin Montiel-Ruiz[1], Exequiel Dellota Jr.[1], Arnold Park[1], Roberto Spreafico[1], Anna Sahakyan[1], Elvin J. Lauron[1], Nadine Czudnochowski[1], Elisabetta Cameroni[1], Sarah Ledoux[1], Adam Werts[3], Christophe Colas[1], Leah Soriaga[1], Amalio Telenti[1], Lisa A. Purcell[1], Seungmin Hwang[1], Gyorgy Snell[1], Herbert W. Virgin[1], Davide Corti[2], Christy M. Hebner[1*]

[1]Vir Biotechnology, San Francisco, California 94158, USA

[2]Humabs Biomed SA, a subsidiary of Vir Biotechnology, 6500 Bellinzona, Switzerland

[3]Lovelace Biomedical, Albuquerque, New Mexico 87108, USA

*corresponding author: chebner@vir.bio

22   ABSTRACT

23   **VIR-7831 and VIR-7832 are dual action monoclonal antibodies (mAbs) targeting the spike**

24   **glycoprotein of severe acute respiratory syndrome coronavirus 2 (SARS-CoV-2). VIR-7831 and**

25   **VIR-7832 were derived from a parent antibody (S309) isolated from memory B cells of a 2003**

26   **severe acute respiratory syndrome coronavirus (SARS-CoV) survivor. Both mAbs contain an "LS"**

27   **mutation in the Fc region to prolong serum half-life and potentially enhance distribution to the**

28   **respiratory mucosa. In addition, VIR-7832 encodes an Fc GAALIE mutation that has been shown**

29   **previously to evoke CD8+ T-cells in the context of an in vivo viral respiratory infection. VIR-7831**

30   **and VIR-7832 potently neutralize wild-type and variant authentic virus in vitro as well as variant**

31   **pseudotyped viruses. In addition, they retain activity against monoclonal antibody resistance**

32   **mutations conferring reduced susceptibility to currently authorized mAbs. The VIR-7831/VIR-**

33   **7832 epitope does not overlap with mutational sites in current variants of concern and continues to**

34   **be highly conserved among circulating sequences consistent with the high barrier to resistance**

35   **observed in vitro. Furthermore, both mAbs can recruit effector mechanisms in vitro that may**

36   **contribute to clinical efficacy via elimination of infected host cells. In vitro studies with these mAbs**

37   **demonstrated no enhancement of infection. In a Syrian golden hamster proof-of concept wildtype**

38   **SARS-CoV-2 infection model, animals treated with VIR-7831 had less weight loss, and significantly**

39   **decreased total viral load and infectious virus levels in the lung compared to a control mAb. Taken**

40   **together, these data indicate that VIR-7831 and VIR-7832 are promising new agents in the fight**

41   **against COVID-19.**

42

43   INTRODUCTION

44   The coronavirus disease (COVID-19) pandemic caused by severe acute respiratory syndrome coronavirus

45   2 (SARS-CoV-2) has resulted in more than 153 million confirmed cases and over 3.2 million deaths

46   worldwide[1]. SARS-CoV-2 infection results in a broad range of disease severity[2]. Infection fatality rates

47   increase significantly with age, with 28.3% of COVID-19 patients over the age of 85 succumbing to

48   disease[2]. However, even in mild-to-moderate COVID-19 patients, significant post-infection sequelae can

49   affect overall health and cause long-term disability[3]. While multiple SARS-CoV-2 vaccines are now

50   authorized for use, issues of supply, vaccine hesitancy and emergence of variants may prevent rapid

51   attainment of herd immunity[4–9]. In addition, there may be individuals who remain at risk despite

52   vaccination due to disease or underlying immunodeficiency. Thus, additional interventions and potential

53   prophylactic agents are needed to reduce morbidity and mortality due to COVID-19.

54   Several monoclonal antibodies (mAbs) targeting the SARS-CoV-2 spike protein have recently been

55   authorized for use in early treatment of COVID-19 patients[10–13] and clinical data have been reported to

56   show promising results in treatment and prophylactic studies[12–15]. However, rapidly spreading variants

57   including those from the United Kingdom (B.1.1.7), South Africa (B.1.351) and Brazil (P.1) exhibit

58   reduced susceptibility in vitro to currently authorized antibodies that target the receptor binding motif

59   (RBM) of the viral spike (S) glycoprotein [10,11,16,17]. Therefore, mAbs targeting unique S epitopes are

60   needed for use alone or in combination with current agents for the treatment and prevention of COVID-

61   19. Furthermore, in addition to viral neutralization, antibodies possessing potent effector function to aid in

62   the killing of virally infected cells and the elicitation of T cell immunity could significantly assist in

63   halting disease progression[18–20].

64   VIR-7831 and VIR-7832 are dual action mAbs derived from the parent antibody S309 identified from a

65   2003 SARS-CoV survivor[21]. These mAbs target an epitope containing a glycan (at position N343) that is

66   highly conserved within the Sarbecovirus subgenus in a region of the S receptor binding domain (RBD)

67   that does not compete with angiotensin converting enzyme 2 (ACE2) binding[22]. This epitope does not

68   overlap with mutations observed in current variants of concern[10,11,16,17]. The variable region of VIR-7831

69   and VIR-7832 have been engineered for enhanced developability. In addition, both antibodies possess an

70   Fc "LS" mutation that confers extended half-life by binding to the neonatal Fc receptor and potentially

71   enhances distribution to the respiratory mucosa [23–25]. VIR-7832 is identical to VIR-7831 with the

72   exception of the addition of a 3 amino acid GAALIE (G236A, A330L, I332E) modification to the Fc

73   domain[26]. The GAALIE modification has previously been shown in vitro to enhance binding to FcγIIa

74   and FcγIIIa receptors, decrease affinity for FcγIIb compared to typical IgG1 and evoke protective CD8+

75   T-cells in the context of viral respiratory infection in vivo [27,28].

76   Here we characterize the antiviral potential of VIR-7831 and VIR-7832. These mAbs effectively

77   neutralize SARS-CoV-2 live virus in vitro as well as in pseudotyped virus assays against emerging

78   variants of concern and variants that confer resistance to currently authorized mAbs[29]. In addition to the

79   neutralizing capacity, both antibodies demonstrate potent effector function and mediate antibody

80   dependent cellular cytotoxicity (ADCC) and antibody dependent cellular phagocytosis (ADCP) in vitro.

81   Furthermore, resistance selection experiments and epitope conservation analyses indicate the potential for

82   a high barrier to resistance. Data derived from the Syrian golden hamster model demonstrates efficacy in

83   a proof-of-concept in vivo model. Taken together, these data indicate that VIR-7831 and VIR-7832 are

84   promising key components of the arsenal in the fight against COVID-19.

85   **RESULTS**

86   **VIR-7831 and VIR-7832 bind SARS-CoV-2 spike and effectively neutralize live virus in vitro.**

87   Previously published work showed that S309 bound SARS-CoV-2 recombinant and cell surface-

88   associated S and neutralized live virus in vitro[21]. We initiated these studies by repeating and extending

89   these earlier results. To determine the binding activity of VIR-7831 and VIR-7832 to the SARS-CoV-2 S,

90   enzyme-linked immunosorbent assay (ELISA), surface plasmon resonance (SPR) and flow cytometry

91   assays were utilized. VIR-7831 and VIR-7832 bound to recombinant S RBD (amino acids 331-541) with

92   EC_{50} values of 20.40 ng/mL and 14.9 ng/mL, respectively, by ELISA (**Figure 1a**). Using SPR, both

93   antibodies demonstrated potent binding to recombinant S RBD with an equilibrium constant (Kd) of 0.21

94   nM (**Figure 1b**). As antibody recognition of cell surface-bound S could mediate killing of virally infected

95   cells, flow cytometry-based studies using cells transiently transfected with a S-encoding plasmid were

96   used to examine antibody binding to cell surface-expressed S trimer. By this method, both VIR-7831 and

97   VIR-7832 bound efficiently to surface-expressed S (**Figure 1c**).

98   To examine neutralization capacity, VIR-7831 and VIR-7832 were tested in a VeroE6 cell-based live

99   SARS-CoV-2 virus system against the Washington 2019 (wild-type) virus as well as against the UK

100   (B.1.1.7), South Africa (B.1.351) and Brazil (P.1) variants. Concentration-dependent viral neutralization

101   of the Washington 2019 strain was observed for both antibodies, with geometric mean $IC_{50/90}$ values of

102   100.1/186.3 ng/mL and 78.3/253.1 ng/mL, respectively (**Figure 1d**). $IC_{50/90}$ values observed for VIR-7831

103   and VIR-7832 against the South Africa and Brazil variant viruses were similar to those against the wild-

104   type strain. A slight shift in the VIR-7831/VIR-7832 $IC_{50/90}$ compared to wild-type was observed for the

105   UK variant. VIR-7831 showed a 3-fold and 4.1-fold shift in IC_{50} and IC_{90}, respectively, against the UK

106   variant compared to wild-type while VIR-7832 had a 3.1-fold shift in IC_{50} and 3.7-fold shift in IC_{90} versus

107   wild-type (**Figure 1d, Table 1**). As variant evolution is a natural part of SARS-CoV-2 biology and

108   emerging live virus variants are not always readily accessible for testing, a vesicular stomatitis virus

109   (VSV)-based pseudotyped virus system targeting Vero E6 cells was used to examine VIR-7831 and VIR-

110   7832 neutralization against emergent variants (**Table 2**). Fold-changes in VIR-7831 and VIR-7832 IC_{50}

111   values compared to wild-type against pseudotyped virus expressing spike from the South Africa, UK or

112   Brazil variant were similar to those observed in the authentic virus system. VIR-7831 was tested against

113   an extended panel of pseudotyped viruses incorporating key variants from around the globe. Fold-changes

114   in VIR-7831 IC_{50} values against these variants ranged from 0.6- to 1.7-fold indicating that VIR-7831

115   retains activity against these spike variants (**Table 2**).

116   **VIR-7831 and VIR-7831 exhibit potent effector function in vitro.** Although direct antiviral

117   mechanisms are crucial to provide protection, Fc-dependent mechanisms mediated by interaction with Fc

118   gamma receptors (FcγRs) on immune cells or with complement, can contribute to overall potency in vivo.

119   The potential for VIR-7831 and VIR-7832 to mediate effector functions were assessed in vitro by

120   measuring binding to FcγRs and C1q and in assays designed to demonstrate antibody-dependent cellular

121   cytotoxicity (ADCC) or antibody-dependent cellular phagocytosis (ADCP)[31–34].

122   Antibody binding to the human activating FcγRIIa (low-affinity R131 and high affinity H131 alleles),

123   FcγRIIIa (low-affinity F158 and high-affinity V158 alleles), and to the inhibitory FcγRIIb were examined

124   using SPR (**Supplemental figure 1a**). VIR-7831 similarly bound both the H131 and R131 alleles of

125   FcγRIIa and binds FcγRIIb. VIR-7831 bound both FcγRIIIa alleles, with reduced binding to the F158

126   allele compared to V158, as is characteristic for human IgG1[35]. Binding of VIR-7831 to C1q was similar

127   to the parental antibody (S309-LS) (**Supplemental figure 1b**). As previously reported for antibodies

128   encoding the GAALIE mutation[26,36], VIR-7832 bound with comparatively higher affinity to activating

129   FcγRIIa and FcγRIIIa than VIR-7831 (**Supplemental figure 1a**). Conversely, VIR-7832 showed reduced

130   affinity for FcγIIb and abrogation of binding to C1q (**Supplemental figure 1b**).

131   The antibodies were also assessed for the ability to activate human FcγRIIa, FcγRIIb or FcγRIIIa, using a

132   Jurkat cell reporter assay[37] (**Figure 2a-d**). S309-GRLR, which contains the effector function-abrogating

133   G236R, L328R mutations was used as a negative control. Cells stably transfected with the SARS-CoV-2

134   spike protein (CHO-CoV-2-Spike) served as target cells. Both VIR-7831 and the parental S309-LS

135   activated signaling of the higher-affinity allele FcγRIIa (H131) but did so less efficiently than the

136   GAALIE-containing antibody VIR-7832 (**Figure 1a**) while VIR-7831, VIR-7832 and S309-LS induced

137   similar low-level activation of the inhibitory receptor FcγRIIb (**Figure 1b**). VIR-7831 demonstrated

138   substantially lower activation of FcγRIIIa F158 versus V158 as expected while VIR-7832 showed

139   increased activation of both alleles of FcγRIIIa (F158 and V158) (**Figures c,d**).

140   To further elucidate the effector function potential of the antibodies, ADCC and ADCP assays were

141   performed using donor PBMCs or NK cells as effector cells and CHO cells stably expressing S (CHO-

142   CoV-2-Spike) as target cells (**Figure 2e-g**). The ability of antibodies to activate NK cell-mediated killing

143   was measured in vitro using two genotyped donors expressing homozygous low-affinity (F/F158) or high-

144   affinity (V/V158) (**Figure 2e-f**). Compared to the parental mAb S309-LS, VIR-7831 had slightly

145   increased capacity to induce NK cell-mediated ADCC when using cells from either F/F158 or V/V158

146   donors. As expected, VIR-7832 induced NK cell-mediated ADCC in cells from donors expressing the

147   low-affinity F/F158 allele of FcγIIIa more efficiently than VIR-7831. These results were confirmed with

148   NK cells from a heterozygous donor (F/V 158).

149   The ability of VIR-7831 and VIR-7832 to facilitate ADCP by primary CD14$^+$ monocytes was measured in

150   vitro by exposing freshly isolated human PBMCs to CHO-CoV-2-Spike cells that were pre-incubated

151   with antibody (**Figure 2g**). VIR-7831, VIR-7832 and S309-LS induced similar levels of ADCP by CD14$^+$

152   monocytes. These results indicate that VIR-7831 and VIR-7832 have the potential to trigger ADCC and

153   ADCP of cells displaying SARS CoV-2 S protein.

154   **Subneutralizing levels of VIR-7831 and VIR-7832 do not enhance virus uptake, replication or**

155   **cytokine production in vitro.** One potential concern with any antibody therapeutic targeting a viral agent

156   is the possibility of antibody-dependent enhancement (ADE). ADE is an in vivo phenomenon in which

157   the presence of an antibody worsens disease. There are several in vitro assays that may provide plausible

158   correlates for ADE in vivo, though none of these have been proven relevant to COVID-19 as to date ADE

159   has not been observed in trials of monoclonal antibodies or plasma[13,15,38,39]. ADE can occur by several

160   potential mechanisms[40]. Poorly neutralizing antibodies or subneutralizing levels of antibody could

161   theoretically facilitate enhanced virus entry and infection through Fc receptor interactions. A second

162   theoretical mechanism involves antibody-antigen complex formation leading to enhanced cytokine

163   production. A third mechanism of ADE has been observed in a porcine model of influenza where the

164   kinetics of viral fusion to the target cell was enhanced in a Fab-dependent manner by fusion-enhancing

165   non-neutralizing antibodies[41,42].

166   To explore whether VIR-7831 and VIR-7832 exhibit in vitro activities that might be related to ADE in

167   vivo, we evaluated SARS-CoV-2 replication in human cells that express FcγRs: monocyte-derived

168   dendritic cells (moDCs), peripheral blood mononuclear cells (PBMCs) and the human U937 macrophage

169   cell line (**Supplemental Figure 2a-b**). Subneutralizing concentrations of VIR-7831 and VIR-7832 were

170   precomplexed with SARS-CoV-2 (MOI =0.01) and added to target cells. Using immunostaining methods,

171   at 24 hours post-infection no productive entry of SARS-CoV-2 into moDCs, PBMCs, or U937 cells was

172   observed in the presence or absence of either mAb, while VeroE6 control cells demonstrated

173   internalization in all conditions evaluated. Reduced internalization of SARS-CoV-2 in VeroE6 cells was

174   observed at the highest concentration of VIR-7831 and VIR-7832 (p-value <0.05), indicating effective

175   virus neutralization prevented virus entry. Using a focus forming assay, virus replication and secretion of

176   infectious virus were detectable by 48 hours post-infection in VeroE6 cells, with comparable levels of

177   replication in the presence or absence of VIR-7831 or VIR-7832. However, no replication of SARS-CoV-

178   2 was detected in moDCs, PBMCs or U937 cells regardless of antibody treatment, indicating lack of

179   productive SARS-CoV-2 infection of these cells, consistent with previously published data[43].

180   To evaluate the potential for VIR-7831 and VIR-7832 to enhance cytokine release upon SARS-CoV-2

181   infection in FcγR-expressing cells, cytokines and chemokines were measured in the supernatants from

182   cells infected with SARS-CoV-2-in the presence of VIR-7831 or VIR-7832 (**Supplemental figure 2c**).

183   Levels of IFN-γ, IL-10, IL-6, IL 8, IP-10, MCP-1, and TNF-α in the supernatant were quantified by MSD

184   at 24- and 48-hours post-infection. For all cell types evaluated, cytokine/chemokine production was

185   similar between all antibody concentrations tested and the no antibody control at both 24- and 48-hours

186   post-infection. Taken together, these in vitro data indicate that neither VIR-7831 nor VIR-7832 exhibit in

187   vitro activities that have been proposed to possibly correlate with ADE in vivo.

188   **VIR-7831 and VIR-7832 have a high barrier to resistance in vitro and do not display cross-**

189   **resistance with other SARS-CoV-2 mAbs.** We next determined whether resistant variants could be

190   elicited by serial passage of SARS-CoV-2 in the presence of VIR-7832. As VIR-7831 and VIR-7832

191   differ only in the Fc region of the antibody, resistance selection experiments were conducted with VIR-

192   7832 as a proxy for both antibodies. SARS-CoV-2 was subjected to 10 passages in the presence of VIR-

193   7832 at fixed concentrations of ~10x, 20x, 50x or 100x IC_{50} (1, 2, 5, or 10 μg/mL) in VeroE6 cells. No

194   CPE was detected in wells passaged with antibody through 10 passages, while CPE was observed in the

195   no antibody control in all passages. Similarly, no virus was detected by focus forming assay at any

196   concentration of VIR-7832 through all 10 passages even at the lowest concentration tested.

197   As no viral breakthrough was observed in the fixed concentration resistance selection, a second method

198   was employed wherein SARS-CoV-2 virus was passaged in sub-IC_{50} concentrations of antibody followed

199   by subsequent passaging in the presence of increasing concentrations of mAb in an attempt to force

200   resistance emergence (**Supplemental Figure 3**). Passaging was performed in duplicate wells to account

201   for founder effects, and concentration increases for each well were based on CPE observations. Five

202   sequential passages were conducted using increasing concentrations of VIR-7832 at 0.5, 1, 2, 5 and ~10x

203   IC_{50} (0.05, 0.1, 0.2, 0.5, 1 µg/mL; **Supplemental Figure 3a**), though no CPE was observed by passages 4

204   and 5 (0.5 and 1 µg/mL, respectively) indicating that variants originally selected at the lower

205   concentrations were either unfit or susceptible to the higher concentrations of antibody. To further assess

206   whether resistance mutations could be generated, selection was restarted using passage 3 virus generated

207   with ~2x IC_{50} (0.2 µg/mL) of VIR-7832 in duplicate wells at ~2x and ~5x IC_{50} (0.2, 0.5 µg/mL),

208   generating two passage lineages (**Supplemental Figure 3b-c**).

209   Supernatants were evaluated for detectable virus at each passage by focus forming assay and cell

210   supernatants from viral passages containing detectable virus were tested in SARS-CoV-2 neutralization

211   assays to evaluate IC_{50} shifts as a marker of reduced susceptibility (**Supplemental Table 1**). With the

212   exception of passage 8, modest fold changes were observed, with shifts in IC_{50} values ranging from 5.4-

213   to 6.5-fold compared to the wild-type SARS-CoV-2 stock virus. In lineage 1, the passage 8 virus

214   displayed a >10-fold shift in IC_{50} (greater than highest concentration tested). Sequence analysis detected

215   an identical 4 amino acid insertion in the N-terminal domain (215-216insKLRS) and 5 amino acid

216   deletion in correspondence of the furin cleavage site (675-679del) in both lineages at all passages

217   sequenced, as well as the amino acid substitution E340A in lineage 1, and R682W, and V1128F in

218   lineage 2. The deletion at amino acids 675-679 has been previously described during passaging of SARS-

219   CoV-2 in tissue culture suggesting enrichment to be a result of cell culture adaptation[44] while the 215-

220   216insKLRS was detected in the input virus. Neither 215-216insKLRS nor R682W variants were highly

221   enriched with passaging (**Supplemental Table 1**) and enrichment of 675-679del and V1128F did not

222   profoundly alter the VIR-7832 IC_{50}. However, appearance of the E340A variant at 98.7% did correlate

223   with a >10-fold shift in IC_{50} suggesting this variant may confer resistance.

224   To evaluate whether amino acid variants identified in the resistance selection conferred reduced

225   susceptibility to VIR-7831 and VIR-7832, neutralization of pseudotyped viruses encoding the S variants

226   was assessed (**Supplemental Table 2**). VIR-7831 and VIR-7832 neutralized R682W and V1128F SARS-

227   CoV-2 pseudotyped virus spike variants with IC_{50} values similar to wild type (< 2-fold change in IC_{50})

228   indicating that these variants do not alter susceptibility. In contrast, E340A conferred reduced

229   susceptibility to VIR-7831 and VIR-7832 (> 100-fold change in IC_{50}) indicating that E340A is a VIR-

230   7831/VIR-7832 monoclonal antibody resistance mutation (MARM).

231   As VIR-7831/VIR-7832 demonstrated a unique in vitro resistance profile, we investigated the potential

232   for cross-resistance to MARMs that confer reduced susceptibility to the authorized monoclonal antibodies

233   bamlanivimab, imdevimab and casirivimab [10,11,45–47] using pseudotyped virus. Notably, some of these

234   mutations are found in highly prevalent variants of concern[17,30,48]. VIR-7831 effectively neutralized

235   pseudotyped viruses expressing spike MARMs that alter bamlanivimab, casirivimab and/or imdevimab

236   activity (**Table 3**). Fold changes in IC_{50} values compared to wild-type were <3-fold for 18/19 variants

237   tested. A modest 3.4-fold shift in the VIR-7831 IC_{50} was observed for the V445A variant that confers

238   reduced susceptibility to imdevimab. These data indicate that VIR-7831/VIR-7832 does not display cross-

239   resistance with currently authorized mAbs and supports the potential combination use of VIR-7831/VIR-

240   7832 with other mAb therapeutics.

241   **The VIR-7831/VIR-7832 epitope is highly conserved among SARS-CoV-2 sequences.** The parental

242   antibody of VIR-7831 and VIR-7832 (S309) binds to a highly conserved sarbecovirus epitope that is

243   potentially intolerant of variation. To investigate the current state of epitope conservation, >1,000,000

244   spike sequences from SARS-CoV-2 deposited in the GISAID database as of April 16, 2021 were

245   examined for epitope variation. More than 99.9% conservation is seen for those amino acids comprising

246   the epitope among currently available sequences for all positions including 17/23 amino acid positions

247   that were ≥99.99 conserved (**Table 4**).

248   VIR-7831 activity against viral mutants carrying single substitutions in the epitope was assessed in

249   pseudotyped virus assays. VIR-7831 effectively neutralized epitope variants at most amino acid positions

250   tested (**Table 5**). Variants at two positions, E340 and P337, resulted in significant IC_{50} shifts indicating

251   reduced susceptibility to VIR-7831. Moderate shifts in potency were observed for P337H and P337T

252   variants (7.50- and 5.38-fold, respective) while more significant shifts in potency were observed for

253   P337L/R and E340A/K/G (27-fold to >276-fold). Notably, these variants are detected in a low number of

254   sequences and do not have a pattern that suggest emergence in the GISAID database (45 and 63 variant

255   counts out of >1,000,000 sequences for P337 and E340, respectively). This observation is consistent with

256   the possibility that variations at these positions come with a fitness cost to the virus.

257   **VIR-7831 reduces weight loss, total viral load and infectious virus levels in a hamster model of**

258   **SARS-CoV-2 infection.** To evaluate the efficacy of VIR-7831 in vivo, the hamster model was utilized.

259   As it was unknown what effect the LS mutation would have in the hamster, a non-LS version of VIR-

260   7831 (SGHmAb-no-LS) was used for these experiments. Hamsters were administered SGHmAb-no-LS

261   intraperitoneally at Day -1 (30, 5, 0.5 or 0.05 mg/kg) or Day -2 (15, 5, 0.5 or 0.05 mg/kg) prior to

262   intranasal SARS-CoV-2 inoculation (**Figure 3a**). Using body weight as a marker of degree of clinical

263   disease, doses of ≥5mg/kg resulted in significantly reduced weight loss at Day 4 compared to controls.

264   (**Figure 3b-e**). Significant decreases in lung viral load were also observed at ≥5mg/kg as measured by

265   RT-qPCR (**Figures f-g**). Day 4 $TCID_{50}$ measurements indicated that antibody administered at ≥0.5 mg/kg

266   resulted in significantly lower levels of infectious virus in lung tissue compared to controls (**Figure 3h-i**).

267   Notably, across these experiments, no enhancement of disease was observed in animals receiving

268   SGHmAb-no-LS based on changes in weight, viral RNA in the lungs, or $TCID_{50}$ infectious virus levels.

269   Collectively, these data indicate that VIR-7831 prevented in a dose-dependent fashion virus replication

270   and morbidity in SARS-CoV-2 challenged hamsters without signs of ADE at any dose tested.

271   **DISCUSSION**

272   Here we show the in vitro and in vivo preclinical characterization of VIR-7831 and VIR-7832, two

273   monoclonal antibodies being advanced into clinical studies[49–51]. Both antibodies demonstrate high-affinity

274   binding to S in vitro, including on the surface of cells, and effectively neutralize wildtype SARS-CoV-2

275   in a live virus assay. VIR-7831 and VIR-7832 retain activity against the UK B.1.1.7, South Africa

276   B.1.351 and Brazil P.1 variants in an authentic virus system, consistent with data using pseudotyped

277   viruses. VIR-7831 bind C1q, activate FcγRs and demonstrate ADCC and ADCP in vitro. Experiments in

278   the hamster model of SARS-CoV-2 infection show proof-of-concept efficacy in vivo. Notably, in vitro

279   and in vivo data did not provide any supporting evidence that these antibodies would demonstrate ADE in

280   a clinical setting.

281   That VIR-7831 and VIR-7832 retain activity against spike variants in authentic virus and pseudotyped

282   virus assays is a key finding at this stage of the pandemic. With the increased transmissibility and

283   potential for more severe disease observed with these viruses, the availability of therapeutic or

284   prophylactic mAbs that remains active against these variants is essential. Current in vitro data indicate

285   that the E484K variant found in both B.1.351, P.1 and other emerging independent lineages, and also

286   recently found in combination with B.1.1.7[52], confers reduced susceptibility to multiple currently

287   authorized monoclonal antibodies possibly lessening the utility of these antibodies or, worse, rendering

288   them ineffective. In addition to retaining activity against key variants of concern, in pseudotyped virus

289   experiments VIR-7831 showed no significant cross-resistance with variants that reduce the activity of

290   authorized mAbs. These data additionally demonstrate the uniqueness of VIR-7831 and VIR-7832 and

291   further highlight the utility VIR-7831 and VIR-7832 could have, alone or in combination, as clinical

292   agents.

293   Notably, even over a year into the pandemic, the VIR-7831/VIR-7832 epitope remains highly conserved

294   among available sequences of circulating virus with ≥99.9% conservation of epitope amino acids. This is

295   consistent with the value of the strategy used for isolation of monoclonal antibodies that neutralize both

296   SARS-CoV and SARS-CoV-2 based on the idea that these two virulent human viruses are

297   phylogenetically divergent within the sarbecovirus subgenus. Furthermore, MARMs identified at

298   positions P337 and E340 are present at very low levels among current sequences. That amino acids P337

299   and E340 remain ≥99.99% conserved at this stage of the pandemic indicates that variants at these

300   positions may confer disadvantageous effects on the virus, consistent with the conservation of this epitope

301   across the sarbecovirus family[21].

302   Viral variants of concern for RBM-targeting mAbs are quickly spreading[53]. The vaccines presently being

303   deployed around the world generate high-titer neutralizing antibodies that target the S protein RBM.

304   Importantly, the RBM is highly immunodominant for responses to natural infection[54]. Vaccine-induced

305   and convalescent immunity may therefore potentially put further mutational pressure on the RBM

306   sequence to evade such antibody responses. In contrast, antibody responses overlapping with the VIR-

307   7831/VIR-7832 epitope are limited after infection [54], possibly because of the shielding effect of the highly

308   conserved N343 glycan. In this regard the epitope may face less vaccine- or infection-generated immune

309   pressure, potentially preserving this conserved epitope long-term.

310   Recent data have indicated that the cells used to generate live virus stocks and overexpression of

311   ACE2/TMPRSS2 in target cells used for assays can affect mAb activity in vitro[29,55]. The VIR-7831/VIR-

312   7832 parental antibody S309 seems particularly sensitive to in vitro methods using ACE2 overexpressing

313   cells[55]. It is therefore notable that VIR-7831 displays significant efficacy in an in vivo proof-of-concept

314   SARS-CoV-2 infection experiment using hamsters despite the fact that patterns of engagement of hamster

315   FcRs by human IgG1 antibodies may not reflect patterns of human IgG1 antibodies with their cognate

316   human FcRs. These findings argue that in vitro data derived from such ACE2 and/or TMPRSS2

317   overexpression cell lines do not accurately reflect the in vivo antiviral capacity of tested mAbs.

318 Furthermore, that the significant in vivo effects of VIR-7831 in the hamster model likely occurred in the

319 absence of full effector functions due to species-specific interactions between antibodies and FcRs, argues

320 that effects in COVID-19 patients incorporating both the neutralization capacity of the antibody plus the

321 ability to harness the strength of the immune system could lead to positive clinical outcomes.

322 The clinical potential of VIR-7832, with the inclusion of the GAALIE Fc mutation, is of special interest

323 in the context of SARS-CoV-2 infection. Previously published data by the Ravetch laboratory comparing

324 the in vivo efficacy of a hemagglutinin-targeting mAb with and without inclusion of the GAALIE

325 mutation in a transgenic humanized FcγR mouse model of influenza infection demonstrated superior

326 efficacy of the GAALIE-containing antibody in both therapeutic and prophylactic experiments[26]. These

327 effects were mediated by protective CD8$^+$ T cell responses elicited by the GAALIE antibody. Clinical

328 data examining the contribution of the adaptive immune response in SARS-CoV-2 infection indicate that

329 poor T cell induction correlates with severe disease (reviewed in [56]). Thus, the potential for VIR-7832 to

330 augment the T cell response to SARS-CoV-2 infection could conceivably play a crucial role in limiting

331 progression to severe COVID-19 disease or in treatment of severe established disease. This latter

332 possibility is supported by recent publications showing that monoclonal antibodies with effector functions

333 are especially effective in the therapeutic setting via recruitment of tissue-protective monocyte functions

334 [19], and that potency of antibodies in the pre-clinical mouse model does not correlate with in vitro

335 neutralizing activity of antibodies[18].

336 Taken together, these data indicate that VIR-7831 and VIR-7832 could play a powerful role in the fight

337 against COVID-19 through the dual action of broadly neutralizing activity paired with engagement of the

338 immune system through effector function capabilities.

339

340

341

METHODS

342

343   **Cells.** Vero E6 cells (ATCC) and Lenti-X 293T cells (Takara) were cultured in Dulbecco's Modified

344   Eagle's medium (DMEM), 10% FBS, 1x Penicillin-Streptomycin at 37°C, 5% CO_2.

345   **Monoclonal Antibodies.** VIR-7831 and VIR-7832 were produced at WuXi Biologics (China). SGHmAb-

346   no-LS, S309-LS, and S309-GRLR were produced at Humabs Biomed SA, a subsidiary of Vir

347   Biotechnology (Bellinzona, Switzerland) in expiCHO cells transiently co-transfected with plasmids

348   expressing the heavy and light chain, as previously described [57].

349   **Virus.** SARS-CoV-2 isolates USA-WA1/2020, UK/VUI/3/2020, hCoV-19/South Africa/KRISP-

350   K005325/2020 and hCoV-19/Japan/TY7-503/2021 were obtained from BEI Resources. To propagate

351   SARS-CoV-2, VeroE6 or VeroE6-TMPRSS2 cells were seeded at $10X10^6$ cells in T175 flasks in growth

352   media and infected the next day at a MOI of 0.001 in virus propagation media. Virus was adsorbed for 1

353   hour at 37°C. Virus inoculum was removed, flasks were washed once with PBS, 25 mL of infection

354   media was added to the cells and flasks were incubated at 37°C. Supernatants were collected at 48 hours

355   post-infection once cytopathic effect was visible, centrifuged at 500 x g for 5 minutes, followed by a

356   second centrifugation at 1000 x g for 5 minutes. Clarified supernatants were then aliquoted and stored at -

357   80°C. Virus titers were determined using a plaque assay on VeroE6 cells, using standard methods.

358   Briefly, 10-fold dilutions of virus stock were incubated in 6 well plates with 2.4% colloidal cellulose

359   overlay for 24 hours. Cells were fixed with 4% PFA for 30 minutes at room temperature (RT),

360   permeabilized with 0.125% Triton X-100, stained with anti-SARS-CoV-2 nucleocapsid antibody at

361   1:5000 and goat anti-rabbit IgG HRP at 1:5000. Plaque forming units (PFU) were visualized with

362   TrueBlue reagent.

363   **In vitro binding ELISA.** For the ELISA assay, 96-well plates were coated with 100 µl/well recombinant

364   SARS-CoV2 RBD diluted in assay diluent (1% BSA/PBS) at a final concentration of 2 µg/mL and

365   incubated overnight at 4°C. Plates were washed three times with 300 µl/well wash buffer using an

366   automated washer. Assay diluent (100 µl/well) was added to block the plates and incubated for 1 hour at

367   room temperature (RT) with shaking. Assay diluent was removed, and plates washed three times with

368   wash buffer. Serial 1:3 dilutions of mAb (concentration range from 6 µg/mL to 0.33 ng/mL) in assay

369   diluent were dispensed at 100 µl/well and incubated 1 hour at RT with shaking, then washed three times

370   with wash buffer. The HRP-conjugated secondary antibody reagent (1:5,000 dilution in assay diluent)

371   was added to each well (100 µl/well) and incubated for 1 hour at RT with shaking. After three washes

372   with wash buffer, 100 µl/well of 2-component TMB peroxidase substrate solution was dispensed in each

373   well and developed for 5 minutes at RT. The reaction was stopped with 100 µL/well 1M H_2SO_4 and the

374   OD was read immediately at 450 nm on a SpectraMax M5 Microplate reader. EC_{50} values were calculated

375   using non-linear regression of log (agonist) versus response in Graph Pad Prism.

376   **Spike binding affinity quantification by SPR.** Antibody was diluted to 2 µg/mL (1 mL) in HBS-EP+

377   buffer and injected at 10 µL/min for 30 seconds across one flow cell of a CM5 sensor chip immobilized

378   with anti-human Fc antibody docked in a Biacore T200. SARS-CoV2-RBD diluted in HBS-EP+ buffer

379   was then injected at a single concentration, 1:3 dilutions from 100 nM to 3.7 nM, across both the flow cell

380   containing captured the antibody as well as a reference flow cell containing only anti-human Fc antibody.

381   Binding was measured with a flow rate of 30 µL/min and an injection time of 600 seconds; dissociation

382   was monitored for 1800 seconds after injection. Data were collected at 10 Hz. After each binding

383   measurement, regeneration reagent was injected to prepare the surface for a new cycle. Experiments were

384   performed at 25°C, with the samples held at 15 °C in the instrument prior to injection.

385   **Measurement of Binding to Human Fcγ Receptors by SPR.** Binding of VIR-7831 and VIR-7832 to

386   human recombinant FcγRs was measured by surface plasmon resonance (SPR) on a Biacore T200.

387   Briefly, Biotin CAPture Reagent (modified streptavidin) was injected across all flow cells of a CAP

388   sensor chip docked in a Biacore T200. Biotinylated Fc receptors at 1 µg/mL were injected across a single

389   flow cell at 10 µL/min for 60 seconds (one receptor per flow cell), with one flow cell reserved as a

390   reference surface. VIR 7831 or VIR-7832 at 100 µg/mL (diluted in HBS-EP+) were injected across all

391   flow cells for 200 seconds using a flow rate of 30 µL/min and association was monitored. Dissociation

392   was monitored for another 200 seconds after injection. Data was collected at 10 Hz. After each binding

393   measurement, CAP Regeneration reagent was injected to prepare the surface for a new cycle.

394   Experiments were performed at 25°C, with the samples held at 15°C in the instrument prior to injection.

395   **Measurement of Binding to Human Complement Protein C1q.** Binding of VIR-7831 and VIR-7832 to

396   human complement was measured by biolayer interferometry (BLI) using an Octet Red96 instrument

397   (FortéBio). Briefly, anti-human Fab (CH1-specific) sensors were used to capture VIR-7831 and VIR-

398   7832 at 10 µg/ml for 10 minutes. The IgG-loaded sensors were then exposed to kinetics buffer containing

399   3 µg/ml of purified human C1q for 4 minutes, followed by a dissociation step in the same buffer for

400   additional 4 minutes. Association and dissociation profiles were measured in real time as changes in the

401   interference pattern.

402   **Binding to Cell Surface Expressed SARS-CoV-2 Spike Protein.** The SARS-CoV-2 spike protein

403   coding sequence (YP_009724390.1, Wuhan-Hu-1 strain) was cloned into a cell expression plasmid under

404   the control of the human CMV promoter (phCMV1) to generate phCMV1 WT spike. ExpiCHO-S cells

405   were seeded the day before transfection at 3×10^6 cells/mL in ExpiCHO Expression Medium.

406   Immediately before transfection, the cells were seeded at 6×10^6 cells cells/mL in a volume of 15 mL in

407   125 mL shake flasks. Six µg of phCMV1 WT spike plasmid or vector control were diluted in 1.2 mL of

408   iced OptiPRO SFM., followed by addition of 48 µL of ExpiFectamine CHO Reagent and complexing for

409   1 minute at RT. The transfection mixture was added dropwise to cells with gentle swirling. Cells were

410   then incubated at 37°C, 8% CO2 with shaking for 42 hours. At 42 hours post-transfection, ExpiCHO-S

411   cells were harvested, washed twice with FACS buffer and resuspended at a concentration of 1.0×10^6

412   cell/mL in PBS. Cells (5×10^4 cells in 50 µl/wells) were dispensed into a 96-well V-bottom plate.

413   Antibody was serially diluted (1:4, 10 points) starting at a concentration of 10 µg/mL. Cells were pelleted

414   at 300 x g for 5 minutes and resuspended in 50 µL/well of antibody serial dilutions and plates were

415   incubated for 45 mins on ice. Cells were washed twice in FACS buffer. Alexa Fluor 647-labelled Goat

416   Anti-Human IgG secondary Ab was diluted 1:750 in FACS buffer and 50 μL was added to the cell pellet

417   for 15 min on ice. Cells were washed twice with FACS buffer, resuspended in 1% PFA. Data was

418   acquired by flow cytometry (CytoFlex LX).

419   **Pseudotyped virus production.** Lenti-X™ 293T cells were seeded in 10-cm dishes for 80% next day

420   confluency. The next day, cells were transfected with the plasmid pcDNA3.1(+)-spike-D19 (encoding the

421   SARS-CoV-2 spike protein) or pcDNA3.1(+)-spike-D19 variants using the transfection reagent TransIT-

422   Lenti according to the manufacturer's instructions. One day post-transfection, cells were infected with

423   VSV-luc (rVSVΔG; Kerafast) at an MOI of 3. The cell supernatant containing SARS-CoV-2 pseudotyped

424   virus was collected at day 2 post-transfection, centrifuged at 1000 x g for 5 minutes to remove cellular

425   debris, aliquoted and frozen at -80°C.

426   **In Vitro Neutralization of SARS-CoV-2 Pseudotyped Virus.** VeroE6 cells were seeded into flat

427   bottom tissue culture 96-well plates at 20,000 cells/well and cultured overnight at 37°C. Twenty-four

428   hours later, 9-point 1:4 serial dilutions of VIR-7831 were prepared in infection medium and each dilution

429   was tested in triplicate per plate (range: 20,000 to 0.3 ng/mL final concentration). SARS-CoV-2 virus

430   stock was diluted in infection media for a final concentration of 2000 plaque forming units per well (MOI

431   0.1). Antibody dilutions were added to virus and incubated for 30 minutes at 37°C. Media was removed

432   from the VeroE6 cells, mAb-virus complexes were added, and cells were incubated at 37°C. At 6 hours

433   post-infection, cells were fixed with 250 μL 4% PFA, incubated for 30 minutes at RT, then washed 3

434   times with PBS to remove residual PFA. The cells were permeabilized with 50 μL of 0.125% Triton X-

435   100 in PBS for 30 minutes at RT. The blocking buffer was removed, 50 μL of SARS-CoV-2 nucleocapsid

436   antibody at 1:2,000 in blocking buffer was added, and plate was incubated for 1 hour at RT. Plates were

437   washed three times with PBS and then incubated for 1 hour at RT with 50 μL/well of goat anti-rabbit-

438   Alexa647 secondary antibody at a final dilution of 1:1,000 mixed with 2 ug/mL Hoechst dye in blocking

439   buffer. After washing 5 times with PBS, 100 μL of fresh PBS was added for imaging. Plates were imaged

440   on a Cytation5 plate reader. Whole well images were acquired (12 images at 4X magnification per well)

441   and nucleocapsid-positive cells were counted using the manufacturer's software.

442   **Live virus neutralization.** VeroE6 cells were seeded into flat bottom tissue culture 96-well plates at

443   20,000 cells/well and cultured overnight at 37°C. Twenty-four hours later, 9-point 1:4 serial dilutions of

444   VIR-7831 were prepared in infection medium and each dilution was tested in triplicate per plate (range:

445   20,000 to 0.3 ng/mL final concentration). SARS-CoV-2 virus stock was diluted in infection media for a

446   final concentration of 2000 plaque forming units per well (MOI 0.1). Antibody dilutions were added to

447   virus and incubated for 30 minutes at 37°C. Media was removed from the VeroE6 cells, mAb-virus

448   complexes were added, and cells were incubated at 37°C. At 6 hours post-infection, cells were fixed with

449   250 µL 4% PFA, incubated for 30 minutes at RT, then washed 3 times with PBS to remove residual PFA.

450   The cells were permeabilized with 50 µL of 0.125% Triton X-100 in PBS for 30 minutes at RT. The

451   blocking buffer was removed, 50 µL of SARS-CoV-2 nucleocapsid antibody at 1:2,000 in blocking buffer

452   was added, and plate was incubated for 1 hour at RT. Plates were washed three times with PBS and then

453   incubated for 1 hour at RT with 50 µL/well of goat anti-rabbit-Alexa647 secondary antibody at a final

454   dilution of 1:1,000 mixed with 2 ug/mL Hoechst dye in blocking buffer. After washing 5 times with PBS,

455   100 µL of fresh PBS was added for imaging. Plates were imaged on a Cytation5 plate reader. Whole well

456   images were acquired (12 images at 4X magnification per well) and nucleocapsid-positive cells were

457   counted using the manufacturer's software..

458   **Determination of Viral Titer by Focus-Forming Assay.** One day prior to infection, 1.2×10^4 VeroE6

459   cells were plated in black-walled, clear bottomed 96-well plates. Virus samples were diluted 1:5 in

460   infection media and adsorbed onto VeroE6 cells for one hour at 37°C. The cells were washed once and

461   overlaid with 1% methylcellulose/serum-containing media. At 24 hours post-infection, the

462   methylcellulose overlay was removed, and cells were washed with PBS. Cells were fixed with 4% PFA,

463   incubated for 30 minutes at RT, then washed with PBS to remove residual PFA. The cells were

464   permeabilized with 50 µL of 0.25% Triton X-100 in PBS for 30 minutes at RT. The Triton X-100 was

465   removed, cells were washed twice with PBS, and incubated with 50 μL of SARS-CoV-2 nucleocapsid

466   antibody at 1:2,000 in blocking buffer for one hour at RT. Plates were washed three times with PBS and

467   then incubated for one hour at RT with 50 μL/well of goat anti-rabbit-Alexa647 secondary antibody at

468   1:1,000 in blocking buffer. After washing three times with PBS, 50 μL of Hoechst dye at 1:1,000 in PBS

469   was added for imaging. Plates were imaged on a Cytation5 plate reader. Whole well images were

470   acquired (12 images at 4X magnification per well) and nucleocapsid-positive foci were counted using the

471   manufacturer's software and used to determine focus-forming units/mL supernatant (FFU/mL).

472   **Determination of mAb-Dependent Activation of Human FcγRIIa, FcγRIIIa or FcγRIIb.** VIR-7831,

473   VIR-7832, S309-LS, and a control mAb with abrogated FcγR binding, S309-GRLR, were serially diluted

474   6-fold in assay buffer from 10,000 ng/ml to 0.006 ng/ml. Nine-point serial dilutions of mAbs were

475   incubated with 12,500 (for FcγRIIIa and FcγRIIb) or 10,000 (for FcγRIIa) CHO-CoV-2-Spike cells per

476   96-plate well in a white, flat-bottom plate for 15 minutes at room temperature. Jurkat effector cells

477   expressing indicated FcγRs and stably transfected with an NFAT-driven luciferase gene were thawed,

478   diluted in assay buffer, and added to the plate at an effector to target cell ratio of 6:1 for FcRγIIIa and

479   FcγRIIb or 5:1 for FcγIIa. Control wells were also included that were used to measure antibody-

480   independent activation (containing target cells and effector cells but no antibody) and background

481   luminescence of the plate (wells containing assay buffer only). Plates were incubated for 18 hours at 37°C

482   with 5% CO2. Activation of human FcγRs in this bioassay results in the NFAT-mediated expression of

483   the luciferase reporter gene. Luminescence was measured with a luminometer after adding the Bio

484   GloTM Luciferase Assay Reagent according to the manufacturer's instructions. To control for

485   background, the mean of the relative luminescence units (RLU) values in wells containing only Assay

486   Buffer was calculated and subtracted from all data points. Data were expressed as the average of RLUs

487   over the background

488   **Determination of NK-Cell Mediated Antibody-Dependent Cellular Cytotoxicity.** Primary NK cell

489   activation was tested using freshly isolated cells from two previously genotyped donors expressing

490   homozygous low affinity (F158) or high affinity (V158) FcγRIIIa. Serial dilutions of mAbs (serially

491   diluted 10-fold in AIM-V Medium from 40,000 ng/ml to 0.075 ng/ml) were incubated with 7,500 CHO-

492   CoV-2 Spike cells per well of a 96 well round-bottom plate for 10 minutes. Target cell and antibody

493   mixtures were then incubated with primary human NK cells as effectors at an effector-to-target ratio of

494   10:1. ADCC was measured using lactate dehydrogenase (LDH) release as a readout according to the

495   manufacturer's instructions (Cytotoxicity Detection Kit (LDH), Roche) after 4 hours of incubation at

496   37°C. In brief, plates were centrifuged for 4 minutes at 400 x g, and 35 µl of supernatant was transferred

497   to a flat 384 well plate. LDH reagent was prepared and 35 µl were added to each well. Using a kinetic

498   protocol, the absorbance at 490 nm and 650 nm was measured once every 2 minutes for 8 minutes, and

499   the slope of the kinetics curve was used as result. The percent specific lysis was determined by applying

500   the following formula: (specific release – spontaneous release) / (maximum release - spontaneous release)

501   x 100.

502   **Determination of Monocyte-Mediated Antibody-Dependent Cellular Phagocytosis.** ADCP assays

503   were performed using human PBMCs freshly isolated from whole blood. CHO CoV-2-Spike cells were

504   used as target cells and were fluorescently labeled with PKH67 Fluorescent Cell Linker Kit (Sigma

505   Aldrich) prior to incubation with mAbs, according to manufacturer's instructions. Serial dilutions of

506   mAbs (serially diluted 5-fold from 5,000 ng/ml to 0.32 ng/ml in RPMI-1640 + L-glutamine supplemented

507   with 10% Hyclone FBS + 2x anti-anti (antibiotic-antimycotic)) were incubated with 10,000 CHO-CoV-2-

508   Spike cells per well of a 96 well polypropylene plate for 10 minutes. Primary PBMCs were fluorescently

509   labeled with Cell Trace Violet according to the manufacturer's instructions. Target cell and antibody

510   mixtures were then incubated with labeled PBMCs at an effector-to-target ratio of 16:1. After an

511   overnight incubation at 37°C, monocytes were stained with anti-human CD14-APC antibody (BD

512   Pharmingen). Antibody-mediated phagocytosis was determined by flow cytometry, gating on CD14+

513   cells that were double positive for cell trace violet and PKH67. Raw data were exported from the flow

514   cytometer into the flow cytometry analysis software FlowJo v10 (Becton Dickinson) for gating and

515   determination of the percentage of $CD14^+$ cells that were also double positive for cell trace violet and

516   PKH67. Cells expressing only cell trace violet or only PKH67 were used to set the positive staining gates.

517   **In vitro resistance selection.** The selection of variants in the presence of increasing concentrations of

518   VIR-7832 was conducted in VeroE6 cells. The day before infection, 6×10^4 VeroE6 cells were seeded in

519   24 well plates and incubated overnight at 37°C. The next day, 600 focus forming units (FFU) of SARS-

520   CoV-2 virus (MOI = 0.01) was incubated with 0.5X IC_{50} of VIR-7832 (0.05 μg/mL) at 37°C for one hour

521   in infection media. The mAb-virus complexes were adsorbed on VeroE6 cells for one hour at 37°C in

522   duplicate wells. After adsorption, cells were washed with DMEM and overlaid with infection media

523   containing 0.05 μg/mL VIR-7832. Control wells infected without antibody were included with each

524   passage. Infected cells were monitored visually for CPE daily. In general, when infected cells exhibited ≥

525   50% CPE, the culture supernatants were harvested, diluted 1:200, and added to fresh VeroE6 cells in 24-

526   well plates with equivalent or increasing concentrations of VIR-7832. At each passage, supernatant was

527   aliquoted and frozen at -80°C for titer and neutralization analyses.

528   **In vitro assessment of potential for ADE.** VeroE6 cells were plated at 1.25×10^4 cells/well one day prior

529   to infection. For each independent experiment, moDCs and PBMCs from five unique moDC donors and

530   six unique PBMC donors were used, with three unique donors used for each independent experiment.

531   Cryopreserved monocytes from unique donors were differentiated into moDCs for six days using human

532   moDC differentiation media according to the manufacturer's protocol. Cryopreserved PBMCs from

533   unique donors are thawed in the presence 0.3 mg/mL DNase and cultured in media for one day prior to

534   infection. On the day of infection, moDCs, PBMCs, and U937 cells were counted and plated at 7.5×10^4

535   cells/well.

536   To examine viral entry, 24 hours post-infection, cells were fixed with 4% PFA, incubated for 30 minutes

537   at RT, then washed with PBS to remove residual PFA. The cells were permeabilized with 50 μL of 0.25%

538   Triton X-100 in PBS for 30 minutes at RT. The Triton X-100 was removed, cells were washed twice with

539   PBS, and incubated with 50 μL of SARS-CoV-2 nucleocapsid antibody at 1:2,000 in blocking buffer for

540   one hour at RT. Plates were washed three times with PBS and then incubated for one hour at RT with 50

541   µL/well of goat anti-rabbit-Alexa647 secondary antibody at 1:1,000 in blocking buffer. After washing

542   three times with PBS, 50 µL of Hoechst dye at 1:1,000 in PBS was added for imaging. Plates were

543   imaged on a Cytation5 plate reader. Whole well images were acquired (12 images at 4X magnification

544   per well) and nucleocapsid-positive cells were counted using the manufacturer's software. The percent of

545   nucleocapsid+ cells was quantified using the Gen5 Imager software (Biotek, Vermont) as number of

546   Cy5+ cells, [(nucleocapsid+ cells)/number of Hoechst+ cells (total cells)]x100. Data was analyzed using

547   Prism v8.00 (GraphPad Software, La Jolla California USA, www.graphpad.com).

548   In order to quantify chemokines and cytokines from supernatants in a BSL2 laboratory, supernatants were

549   inactivated by 10 minutes exposure to UVC light at 5,000 µJ/cm2. Supernatants were diluted 1:5 in

550   infection media and levels of cytokines/chemokines were quantified using the U-plex 96-well assay

551   according to the manufacturer's protocol (Meso Scale Diagnostics, Rockville, MD). Quantification of

552   cytokines and chemokines were determined based on an 8-point standard curve in duplicate, provided by

553   the manufacturer. Cytokine data was analyzed using the Discovery Workbench v4.0.13 software (Meso

554   Scale Diagnostics). Data was graphed and statistical analyses were conducted using Prism software.

555   **Sequencing of SARS-CoV-2 Spike Gene.** To isolate nucleic acid from the supernatant of viral passages,

556   120 µL of cell supernatant was added to 360 µL of Trizol and stored at -80°C for further analysis. Trizol

557   collected samples from viral passages where a shift in neutralization > 2-fold relative to wild type was

558   detected were subjected to RNA isolation using PureLink RNA Mini Kit with the incorporation of on-

559   column PureLink DNase Treatment, following manufacturer's instructions. Reverse transcription

560   reactions were performed with 6 µL of purified RNA and oligoT primers using the NEB ProtoScript II

561   First Strand cDNA Synthesis kit, according to manufacturer's instructions. The resulting cDNA was used

562   as a template for PCR amplification of the spike gene using the KapaBiosystems polymerase (KAPA HiFi

563   HotStart ReadyMix) with primers 5' aattatcttggcaaaccacg-3' and 5' tgaggcttgtatcggtatcg-3'.

564   Amplification conditions included an initial 3 minutes at 95°C, followed by 28 cycles with 20 seconds at

565   98°C, 15 seconds at 62°C and 72°C for 2 minutes, with a final 4 minutes at 72°C. PCR products were

566   purified using AMPure XP beads following manufacturer's instructions. The size of the amplicon was

567   confirmed by analyzing 2 μL of PCR products using the Agilent D5000 ScreenTape System. Products

568   were quantified by analyzing 1 μL with the Quant-iT dsDNA High-Sensitivity Assay Kit. Twenty ng of

569   purified PCR product was used as input for library construction using the NEBNext Ultra II FS DNA

570   Library Prep kit following manufacturer's instructions. DNA fragmentation was performed for 13

571   minutes. NEBNext Multiplex Oligos for Illumina Dual Index Primer Set 1 was used for library

572   construction, with a total of 6 PCR cycles. Libraries size was determined using the Agilent D1000

573   ScreenTape System and quantified with the Quant iT dsDNA High-Sensitivity Assay Kit. Equal amounts

574   of each library were pooled together for multiplexing and 'Protocol A: Standard Normalization Method'

575   of the Illumina library preparation guide was used to prepare 8 pM final multiplexed libraries with 1%

576   PhiX spike-in for sequencing. The MiSeq Reagent Kit v3 (600-cycle) was used for sequencing the

577   libraries on the Illumina MiSeq platform, with 300 cycles for Read 1, 300 cycles for Read 2, 8 cycles for

578   Index 1, and 8 cycles for Index 2.

579   **Bioinformatics Analysis of Conservation.** Available genome sequences for SARS-CoV-2 were

580   downloaded from Global Initiative on Sharing All Influenza Data (GISAID; https://www.gisaid.org/) on

581   April 16, 2021. Bat and pangolin sequences were removed to yield human-only sequences. The spike

582   open reading frame was localized by aligning the reference protein sequence (NCBI reference sequence:

583   YP_009724390.1) to the genomic sequence of isolates with Exonerate v.2.4.0. Coding nucleotide

584   sequences were translated in silico using seqkit v.0.12.0. Multiple sequence alignment was performed

585   using MAFFT v.7.455. Variants were determined by comparison of aligned sequences to the reference

586   sequence using the R v3.6.3/Bioconductor v.3.10 package Biostrings v.2.54.0.

587   **In vivo studies.** Syrian golden hamster studies were conducted at Lovelace Biomedical (Albuquerque,

588   NM). Twelve- to sixteen-week-old male hamsters were interperitoneally administered a non-LS version

589   of VIR-7831 (SGHmAb-no-LS), control antibody or diluent Day -1 or Day -2 prior to virus challenge.

590 Animals were inoculated intranasally at Day 0 with 7.4×10^4 TCID$_{50}$ with SARS-CoV-2 (isolate USA-

591 WA1/2020). Animals were also weighed once daily in the morning beginning on study Day -10 and

592 continuing until the end of the study. Following euthanasia, RT-qPCR was performed on lung

593 homogenates using quantitative real-time PCR methods targeting the SARS-CoV-2 N gene and the

594 median tissue culture infections dose (TCID$_{50}$) was determined per Lovelace internal methodology.

Author Contributions

596 Conceived studies: A.L.C, C.H-D., F.A.P, D.M., M.S., L.S., A.T., L.A.P., S.H., G.S., H.W.V., D.C., C.M.H.

597 Designed studies and experiments: A.L.C, C.H.D., F.A.P, D.M., M.S., M.L.A., E. D., B.G., J.D., L.R.,A.C., A.S.,

598 R.S., J.W., N.C., E.C., S.L., C.C., D.P., C.S., J.N., A.P., A.W., L.S., A.T., L.A.P., S.H., G.S., H.W.V., D.C., C.M.H.

599 Performed experiments: D.M., M.S., M.L.A., B.G., J.D., E.D., A.S., L.R., H.T., J.D., S.S., D.P., C.S., J.N., B.S.,

600 S.B., J.W., J.Z., H.K., A.C., M.M-R., A.P., A.W., N.C., E.C. Analyzed and interpreted data: A.L.C., C.H-D., F.A.L.,

601 D.M., M.S., M.L.A., B.G., J.D., D.P., C.S., J.N., E.L., A.S., R.S., L.R., H.T., B.S., S.B., J.W., J.Z., H.K., A.C., M. M-

602 R., N.C., E.C., S.L., A.W., C.C., L.S., A.T., S.H., G.S., H.W.G, D.C., C.M.H. Prepared the manuscript with input

603 from all authors: A.L.C., G.S., A.T., L.P., D.C., H.W.G., C.M.H.

Competing interests

605 Some authors are current or former employees of Vir Biotechnology or Humabs BioMed SA (a fully-

606 owned subsidiary of Vir Biotechnology) and may hold shares in Vir Biotechnology. H.W.V. is a founder of

607 PierianDx and Casma Therapeutics.

608

REFERENCES

1. WHO Coronavirus Disease (COVID-19) Dashboard | WHO Coronavirus Disease (COVID-19) Dashboard. https://covid19.who.int/.

2. Levin, A. T. *et al.* Assessing the age specificity of infection fatality rates for COVID-19: systematic review, meta-analysis, and public policy implications. *Eur J Epidemiol* **35**, 1123–1138 (2020).

3. Dennis, A. *et al.* Multi-organ impairment in low-risk individuals with long COVID. doi:10.1101/2020.10.14.20212555.

4. Murphy, J. *et al.* Psychological characteristics associated with COVID-19 vaccine hesitancy and resistance in Ireland and the United Kingdom. *Nat Commun* **12**, 29 (2021).

5. Khubchandani, J. *et al.* COVID-19 Vaccination Hesitancy in the United States: A Rapid National Assessment. *J Commun Health* 1–8 (2021) doi:10.1007/s10900-020-00958-x.

6. Sallam, M. *et al.* High Rates of COVID-19 Vaccine Hesitancy and Its Association with Conspiracy Beliefs: A Study in Jordan and Kuwait among Other Arab Countries. *Nato Adv Sci Inst Se* **9**, 42 (2021).

7. Tegally, H. *et al.* Emergence and rapid spread of a new severe acute respiratory syndrome-related coronavirus 2 (SARS-CoV-2) lineage with multiple spike mutations in South Africa. *medRxiv* (2020) doi:10.1101/2020.12.21.20248640.

8. Naveca, F. *et al.* Phylogenetic relationship of SARS-CoV-2 sequences from Amazonas with emerging Brazilian variants harboring mutations E484K and N501Y in the Spike protein - SARS-CoV-2 coronavirus / nCoV-2019 Genomic Epidemiology - Virological. https://virological.org/t/phylogenetic-relationship-of-sars-cov-2-sequences-from-amazonas-with-emerging-brazilian-variants-harboring-mutations-e484k-and-n501y-in-the-spike-protein/585 (2011).

9. Rambaut, A. *et al.* Preliminary genomic characterisation of an emergent SARS-CoV-2 lineage in the UK defined by a novel set of spike mutations - SARS-CoV-2 coronavirus / nCoV-2019 Genomic Epidemiology - Virological. https://virological.org/t/preliminary-genomic-characterisation-of-an-emergent-sars-cov-2-lineage-in-the-uk-defined-by-a-novel-set-of-spike-mutations/563 (2020).

10. Bamlanivimab EUA Letter of Authorization Reissue 02092021. https://www.fda.gov/media/143603/download.

11. Casirivimab and Imdevimab EUA Fact Sheet for Healthcare Providers. https://www.fda.gov/media/143892/download.

643 12. Lilly's neutralizing antibody bamlanivimab (LY-CoV555) prevented COVID-19 at nursing
644 homes in the BLAZE-2 trial, reducing risk by up to 80 percent for residents.
645 https://investor.lilly.com/node/44291/pdf.

646 13. Gottlieb, R. L. *et al.* Effect of Bamlanivimab as Monotherapy or in Combination With
647 Etesevimab on Viral Load in Patients With Mild to Moderate COVID-19. *Jama* **325**, 632–644
648 (2021).

649 14. Chen, P. *et al.* SARS-CoV-2 Neutralizing Antibody LY-CoV555 in Outpatients with Covid-
650 19. *New Engl J Med* (2020) doi:10.1056/nejmoa2029849.

651 15. Weinreich, D. M. *et al.* REGN-COV2, a Neutralizing Antibody Cocktail, in Outpatients with
652 Covid-19. *New Engl J Med* **384**, 238–251 (2020).

653 16. Starr, T. N. *et al.* Prospective mapping of viral mutations that escape antibodies used to treat
654 COVID-19. *Science* **371**, 850–854 (2021).

655 17. Wang, P. *et al.* Increased Resistance of SARS-CoV-2 Variants B.1.351 and B.1.1.7 to
656 Antibody Neutralization. *Biorxiv* 2021.01.25.428137 (2021) doi:10.1101/2021.01.25.428137.

657 18. Schäfer, A. *et al.* Antibody potency, effector function, and combinations in protection and
658 therapy for SARS-CoV-2 infection in vivo. *J Exp Med* **218**, (2020).

659 19. Winkler, E. S. *et al.* Human neutralizing antibodies against SARS-CoV-2 require intact Fc
660 effector functions and monocytes for optimal therapeutic protection. *Biorxiv* 2020.12.28.424554
661 (2020) doi:10.1101/2020.12.28.424554.

662 20. Bournazos, S. & Ravetch, J. V. Fcγ Receptor Function and the Design of Vaccination
663 Strategies. *Immunity* **47**, 224–233 (2017).

664 21. Pinto, D. *et al.* Cross-neutralization of SARS-CoV-2 by a human monoclonal SARS-CoV
665 antibody. *Nature* **583**, 290–295 (2020).

666 22. Pinto, D. *et al.* Cross-neutralization of SARS-CoV-2 by a human monoclonal SARS-CoV
667 antibody. *Nature* **583**, 290–295 (2020).

668 23. Ko, S.-Y. *et al.* Enhanced neonatal Fc receptor function improves protection against primate
669 SHIV infection. *Nature* **514**, 642 (2014).

670 24. Zalevsky, J. *et al.* Enhanced antibody half-life improves in vivo activity. *Nat Biotechnol* **28**,
671 157 (2010).

672 25. Gaudinski, M. R. *et al.* Safety and pharmacokinetics of the Fc-modified HIV-1 human
673 monoclonal antibody VRC01LS: A Phase 1 open-label clinical trial in healthy adults. *Plos Med*
674 **15**, e1002493 (2018).

675   26. Bournazos, S., Corti, D., Virgin, H. W. & Ravetch, J. V. Fc-optimized antibodies elicit CD8
676   immunity to viral respiratory infection. *Nature* 1–9 (2020) doi:10.1038/s41586-020-2838-z.

677   27. Weitzenfeld, P., Bournazos, S. & Ravetch, J. V. Antibodies targeting sialyl Lewis A mediate
678   tumor clearance through distinct effector pathways. *J Clin Invest* **129**, 3952–3962 (2019).

679   28. Bournazos, S., Corti, D., Virgin, H. W. & Ravetch, J. V. Fc-optimized antibodies elicit CD8
680   immunity to viral respiratory infection. *Nature* 1–9 (2020) doi:10.1038/s41586-020-2838-z.

681   29. Diamond, M. *et al.* SARS-CoV-2 variants show resistance to neutralization by many
682   monoclonal and serum-derived polyclonal antibodies. *Res Square* (2021) doi:10.21203/rs.3.rs-
683   228079/v1.

684   30. Chen, R. E. *et al.* Resistance of SARS-CoV-2 variants to neutralization by monoclonal and
685   serum-derived polyclonal antibodies. *Nat Med* 1–10 (2021) doi:10.1038/s41591-021-01294-w.

686   31. Kallewaard, N. L. *et al.* Structure and Function Analysis of an Antibody Recognizing All
687   Influenza A Subtypes. *Cell* **166**, 596–608 (2016).

688   32. DiLillo, D. J., Tan, G. S., Palese, P. & Ravetch, J. V. Broadly neutralizing hemagglutinin
689   stalk–specific antibodies require FcγR interactions for protection against influenza virus in vivo.
690   *Nat Med* **20**, 143–151 (2014).

691   33. Dunand, C. J. H. *et al.* Both Neutralizing and Non-Neutralizing Human H7N9 Influenza
692   Vaccine-Induced Monoclonal Antibodies Confer Protection. *Cell Host Microbe* **19**, 800–813
693   (2016).

694   34. Leon, P. E. *et al.* Optimal activation of Fc-mediated effector functions by influenza virus
695   hemagglutinin antibodies requires two points of contact. *Proc National Acad Sci* **113**, E5944–
696   E5951 (2016).

697   35. Bruhns, P. *et al.* Specificity and affinity of human Fcγ receptors and their polymorphic
698   variants for human IgG subclasses. *Blood* **113**, 3716–3725 (2009).

699   36. Weitzenfeld, P., Bournazos, S. & Ravetch, J. V. Antibodies targeting sialyl Lewis A mediate
700   tumor clearance through distinct effector pathways. *J Clin Invest* **129**, 3952–3962 (2019).

701   37. Cheng, Z. J. *et al.* Development of a robust reporter-based ADCC assay with frozen, thaw-
702   and-use cells to measure Fc effector function of therapeutic antibodies. *J Immunol Methods* **414**,
703   69–81 (2014).

704   38. Arvin, A. M. *et al.* A perspective on potential antibody-dependent enhancement of SARS-
705   CoV-2. *Nature* 1–11 (2020) doi:10.1038/s41586-020-2538-8.

706   39. Joyner, M. J. & Wright, R. S. Safety Update: CO VID-19 Convalescent Plasma in
707   20,000 Hospitalized Patients. *Mayo Clinic Proceedings* (2020).

708   40. Arvin, A. M. *et al.* A perspective on potential antibody-dependent enhancement of SARS-
709   CoV-2. *Nature* **584**, 353–363 (2020).

710   41. Khurana, S. *et al.* Vaccine-induced anti-HA2 antibodies promote virus fusion and enhance
711   influenza virus respiratory disease. *Sci Transl Med* **5**, 200ra114 (2013).

712   42. Winarski, K. L. *et al.* Antibody-dependent enhancement of influenza disease promoted by
713   increase in hemagglutinin stem flexibility and virus fusion kinetics. *Proc National Acad Sci* **116**,
714   15194–15199 (2019).

715   43. Hui, K. P. Y. *et al.* Tropism, replication competence, and innate immune responses of the
716   coronavirus SARS-CoV-2 in human respiratory tract and conjunctiva: an analysis in ex-vivo and
717   in-vitro cultures. *Lancet Respir Medicine* (2020) doi:10.1016/s2213-2600(20)30193-4.

718   44. Liu, Z. *et al.* Identification of Common Deletions in the Spike Protein of Severe Acute
719   Respiratory Syndrome Coronavirus 2. *J Virol* **94**, (2020).

720   45. Baum, A. *et al.* Antibody cocktail to SARS-CoV-2 spike protein prevents rapid mutational
721   escape seen with individual antibodies. *Science* **369**, 1014–1018 (2020).

722   46. Thomson, E. C. *et al.* Circulating SARS-CoV-2 spike N439K variants maintain fitness while
723   evading antibody-mediated immunity. *Cell* (2021) doi:10.1016/j.cell.2021.01.037.

724   47. Starr, T. N., Greaney, A. J., Dingens, A. S. & Bloom, J. D. Complete map of SARS-CoV-2
725   RBD mutations that escape the monoclonal antibody LY-CoV555 and its cocktail with LY-
726   CoV016. doi:10.1101/2021.02.17.431683.

727   48. Wise, J. Covid-19: The E484K mutation and the risks it poses. *Bmj* **372**, n359 (2021).

728   49. VIR-7831 for the Early Treatment of COVID-19 in Outpatients - Full Text View -
729   ClinicalTrials.gov. https://clinicaltrials.gov/ct2/show/NCT04545060?term=VIR-
730   7831&draw=2&rank=2.

731   50. A Study of Immune System Proteins in Participants With Mild to Moderate COVID-19
732   Illness - Full Text View - ClinicalTrials.gov.
733   https://clinicaltrials.gov/ct2/show/NCT04634409?term=VIR-7831&draw=2&rank=3.

734   51. Vir Biotechnology and GSK announce NHS-supported AGILE study to evaluate VIR-7832
735   in the early treatment of COVID-19 | GSK. *undefined* https://www.gsk.com/en-gb/media/press-
736   releases/vir-biotechnology-and-gsk-announce-nhs-supported-agile-study-to-evaluate-vir-7832-
737   in-the-early-treatment-of-covid-19/.

738   52. Wise, J. Covid-19: New coronavirus variant is identified in UK. *Bmj* **371**, m4857 (2020).

739   53. CoVariants. https://covariants.org/.

740   54. Piccoli, L. *et al.* Mapping neutralizing and immunodominant sites on the SARS-CoV-2 spike
741   receptor-binding domain by structure-guided high-resolution serology. *Cell* (2020)
742   doi:10.1016/j.cell.2020.09.037.

743   55. Rappazzo, C. G. *et al.* Broad and potent activity against SARS-like viruses by an engineered
744   human monoclonal antibody. *Science* **371**, 823–829 (2021).

745   56. Sette, A. & Crotty, S. Adaptive immunity to SARS-CoV-2 and COVID-19. *Cell* **184**, 861–
746   880 (2021).

747   57. Stettler, K. *et al.* Specificity, cross-reactivity and function of antibodies elicited by Zika virus
748   infection. *Science* **353**, aaf8505 (2016).

749

750   **FIGURE LEGENDS**

751   **Figure 1.** VIR-7831 and VIR-7831 bind S and neutralize SARS-CoV-2 virus and S variants of concern in

752   vitro. a) Binding of VIR-7831 (black circles) and VIR-7832 (blue squares) to SARS-CoV-2 RBD was

753   tested by ELISA. Shown is the average of four replicates and SD derived from three independent

754   experiments. b) Association and dissociation profiles of VIR-7831 to SARS-CoV-2-RBD were measured

755   using SPR. The double reference subtracted curves (shown for single replicates) are plotted together with

756   the curve fit in black (obscured by close overlay with the data). Values are from two independent

757   experiments. c) Binding of VIR-7831 (black circles) and VIR-7832 (blue squares) to cell-surface S

758   protein was determined by flow cytometry. Data are expressed as the percentage of the positive cells.

759   Results shown are from one experiment and representative of three independent experiments performed.

760   d) In vitro neutralization of live SARS-CoV-2 by different concentrations of VIR-7831 (left) and VIR-

761   7832 (right) measured by nucleocapsid staining 6-hours post-infection. Results shown are from one

762   experiment and representative of at least three independent experiments performed.

763   **Figure 2.** VIR-7831 and VIR-7832 demonstrate effector function in vitro. In vitro effector function (a-e)

764   activation profiles of human FcγRIIa (a), FcγRIIb (b), FcγRIIIa low-affinity (F158) (c) or FcγRIIIa high-

765   affinity binding allele (V158) (d) using bioreporter assays using S-expressing CHO cells as the target

766   antigen. Data points show means± SD of duplicates. NK-cell mediated killing (ADCC) of S-expressing

767   CHO cells using freshly isolated cells from two donors previously genotyped for homozygous expression

768   of low-affinity (F/F158) (e) or high-affinity (V/V158) FcγRIIIa (f). Data points are means of

769   quadruplicates ± SD. g) Antibody-dependent cellular phagocytosis (ADCP) using S-expressing CHO cells

770   and freshly isolated PBMCs. Data represent the means of duplicates ± SD.

771   **Figure 3.** VIR-7831 shows in vivo efficacy in a hamster SARS-CoV-2 model of infection. a) Overview

772   of hamster in vivo study design. b) and c) Animal weight over time as a percent of starting weight in

773   animals dosed a Day -1 (b) or Day -2 (c). Medians of at least N=6 animals and interquartile range are

774   shown. d) and e) Day 4 terminal weights expressed as a percentage of starting weight for animals dosed at

775   Day -1 (d) or Day -2 (e). Bar denotes median values. f) and g) Day 4 lung viral load in Day -1 (f) or Day -

776   2 (g) treated animals as assessed by RT-qPCR. Bar denotes median values. h) and i) infectious virus in

777   lung at Day 4 for Day -1 (h) or Day -2 (i) dosed animals. Bar denotes median values. ns=not significant,

778   ** = p<0.05, and *** = <0.005 as assessed by the Mann-Whitney U-test.

779   **Table 1.** VIR-7831 and VIR-7832 retain activity against S variants of concern in an authentic virus

780   system**.** Average fold change in VIR-7831 and VIR-7832 IC_{50} compared to relative wild-type controls for

781   S variants tested in an authentic virus system. Data shown are averages of at least two independent

782   experiments.

783   **Table 2.** VIR-7831 and VIR-7832 retain activity against S variants of concern in a pseudotyped virus

784   system**.** Average fold change in VIR-7831 and VIR-7832 IC_{50} compared to relative wild-type controls for

785   S variants tested in a VSV/VeroE6 pseudotyped virus system. Data shown are averages of at least two

786   independent experiments.

787   **Table 3.** VIR-7831 and VIR-7832 retain activity against variants that confer resistance to authorized

788   mAbs. Activity of VIR-7831 against variants conferring reduced susceptibility to bamlanivimab,

789   imdevimab or casirivimab in a VSV/VeroE6 pseudotyped virus system. The geometric mean of IC_{50}s and

790   average fold-change versus the relative wild-type control from at least two independent experiments are

791   shown.

792   **Table 4.** The VIR-7831/VIR-7832 epitope is highly conserved. Conservation data comprising >1,000,000

793   sequences from the GISAID database and variants at each position are shown. Variants in bold were

794   tested in a pseudotyped virus assay.

795   **Table 5.** Activity of VIR-7831 against epitope variants. VIR-7831/VIR-7832 epitope variants detected in

796   sequences from the GISAID database were tested in a VSV/VeroE6 pseudotyped virus system. The

797   geometric mean of IC_{50}s and average fold-change versus the relative wild-type control from at least two

798   independent experiments are shown. Variants marked with "a" indicates that the data shown are from the

799   parental antibody S309.

800   **Supplemental Figure 1.** Binding of VIR-7831 and VIR-7832 to human FcγRs and C1q as measured by

801   SPR. Binding of VIR-7831 and VIR-7832 to a) human FcγRIIa (H131 and R131 alleles), FcγRIIIa (F158

802   and V158 alleles) and FcγRIIb were measured using SPR. Biotinylated purified FcγRs were captured on

803   the sensor chip surface prior to injection of VIR-7831 or VIR-7832. Association and dissociation profiles

804   (separated by the vertical dotted line) were measured in real time as change in the SPR signal. b) Binding

805   of VIR-7831 and VIR-7832 to complement component C1q was measured using BLI on an Octet Red96

806   instrument. Association and dissociation profiles (separated by the vertical dotted line) were measured in

807   real time as change in the interference pattern.

808   **Supplemental Figure 2.** Sub-neutralizing concentrations of VIR-7831 and VIR-7832 do not enhance

809   viral entry, viral replication or cytokine production in vitro. Internalization (a) and replication (b) of

810   SARS-CoV-2 was evaluated in VeroE6, moDCs or PBMCs at various timepoints. Two independent

811   experiments with human moDCs and PBMCs from three individual donors were analyzed (5 unique

812   moDC donors, 6 unique PBMC donors total between two experiments). VeroE6 cells were run in

813   duplicate for both independent experiments. Data from each replicate well from two independent

814   experiments are plotted as individual points, with horizontal lines representing the median. Mann-

815   Whitney U-test comparison to no antibody group, *p<0.05. c) Supernatant cytokine and chemokine levels

816   as measured by MSD at the indicated time post infection. Data from two independent experiments (three

817   replicates each, five unique donors) are plotted as the mean and SD.

818   **Supplemental Figure 3.** Overview of VIR-7832 resistance selection method. All passaging was

819   conducted in duplicate wells. (a) VIR-7832 concentration was increased during each passage. P3 X

820   indicates passage 3 virus, after which virus was lost with subsequent increases in concentration. In (b) and

821   (c), p3X denotes where passage 3 virus from (a) was used to initiate (b) viral lineage 1 and (c) viral

822   lineage 2. Arrows indicate passages that were subjected to sequence analysis, and * indicate the passages

823   in lineage 1 with no detectable virus or CPE. Selection continued for a total of eight passages.

824   **Supplemental Table 1.** Amino acid substitutions identified in the SARS-CoV-2 S upon in vitro selection

825   with VIR-7832. Spike gene sequences were compared to a SARS-CoV-2 reference sequence (NCBI:

826   NC_045512.2) to identify variants. Fold-changes in IC_{50} were determined compared to the SARS-CoV-2

827   virus stock.

828   **Supplemental Table 2.** VIR-7831 and VIR-7832 activity against selected S variants. VIR-7831/VIR-

829   7832 epitope variants observed by in vitro resistance selection were individually tested in a VSV/VeroE6

830   pseudotyped virus system. The geometric mean of IC_{50}s and average fold-change versus the relative wild-

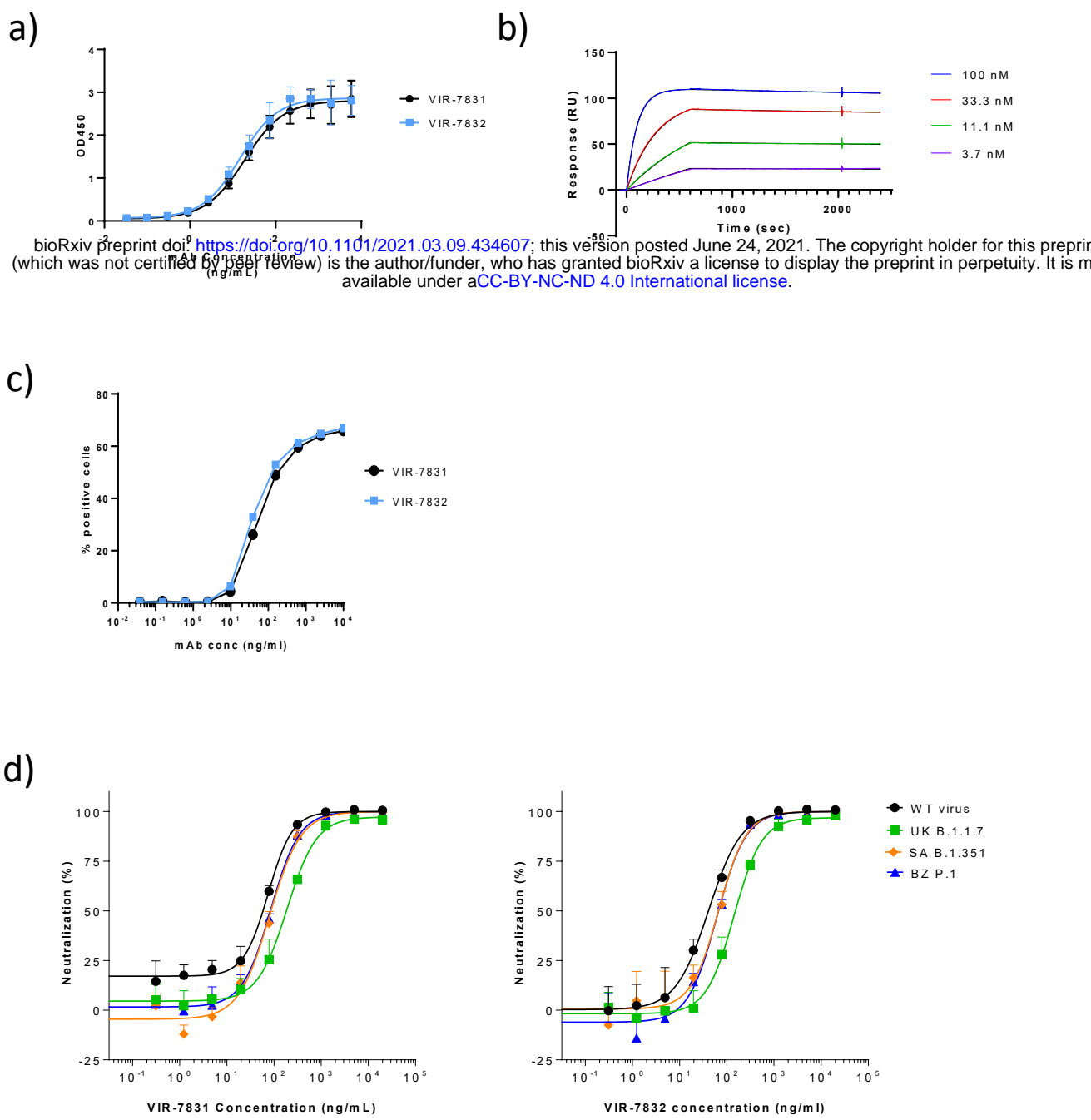831   type control from at least two independent experiments are shown.
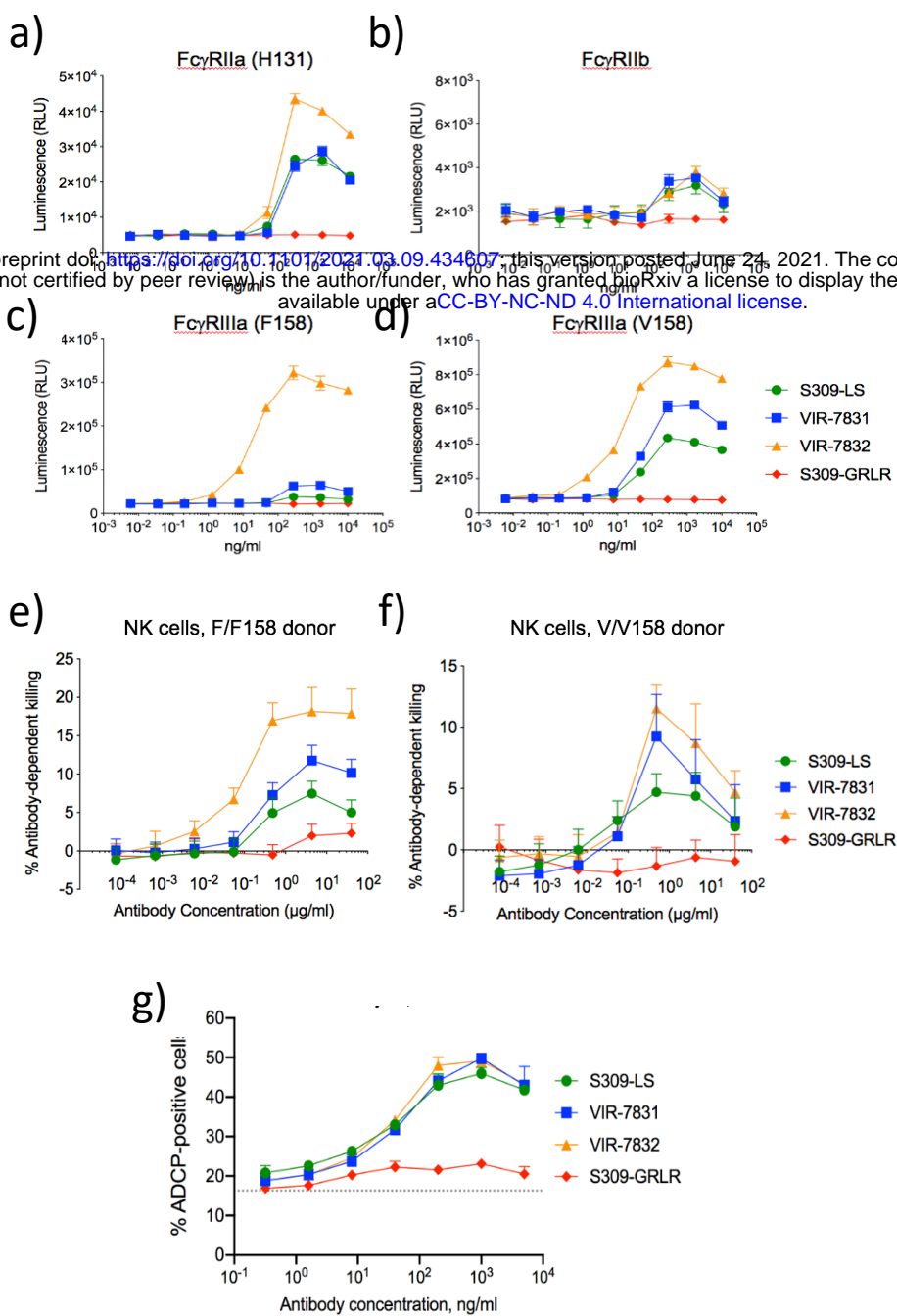
832

Figure 1

a)

b)

c)

d)

Figure 2

a)

FcγRIIa (H131)

b)

FcγRIIb

c)

FcγRIIIa (F158)

d)

FcγRIIIa (V158)

- ● S309-LS
- ■ VIR-7831
- ▲ VIR-7832
- ◆ S309-GRLR

e)

NK cells, F/F158 donor

f)

NK cells, V/V158 donor

- ● S309-LS
- ■ VIR-7831
- ▲ VIR-7832
- ◆ S309-GRLR

g)

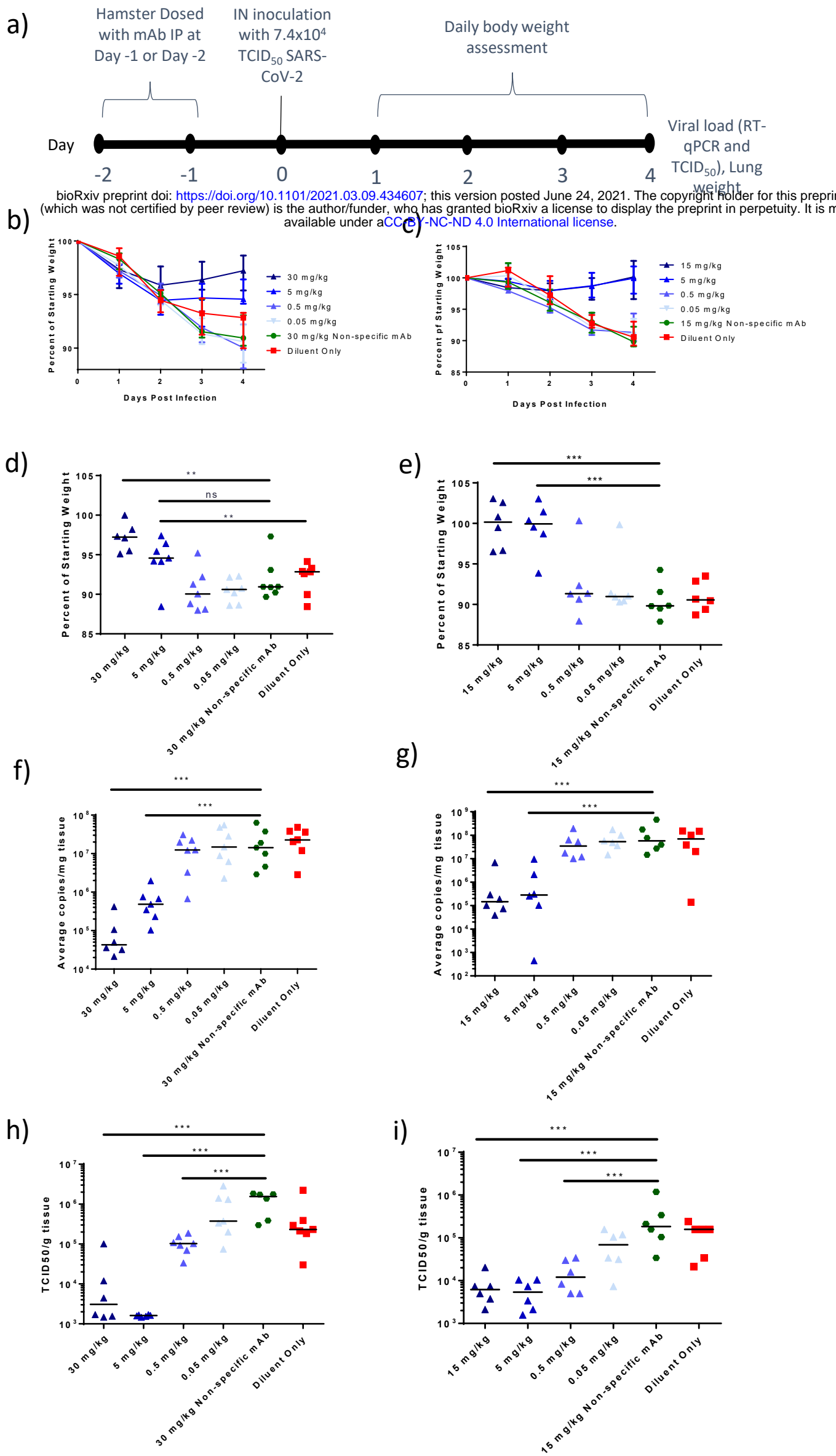- ● S309-LS
- ■ VIR-7831
- ▲ VIR-7832
- ◆ S309-GRLR

Figure 3

Table 1

SARS-CoV-2 Variant	Geometric Mean VIR-7831 IC_{50} (ng/ml) (Average Fold Change IC_{50} vs. Wild-Type)	Geometric Mean VIR-7831 IC_{90} (ng/ml) (Average Fold Change IC_{90} vs. Wild-Type)	Geometric Mean VIR-7832 IC_{50} (ng/ml) (Average Fold Change IC_{50} vs. Wild-Type)	Geometric Mean VIR-7832 IC_{90} (ng/ml) (Average Fold Change IC_{90} vs. Wild-Type)
UK (B.1.1.7)	187.15 (3.0)	1246.86 (4.1)	181.12 (3.1)	1222.95 (3.7)
South Africa (B.1.351)	71.89 (1.2)	385.01 (1.3)	59.67 (1.1)	309.84 (0.9)
Brazil (P.1)	73.11 (1.6)	335.79 (1.4)	48.94 (1.2)	217.02 (0.9)

Table 2

Variant	Spike Mutations	Fold-Change in VIR-7831 IC_{50} vs. Wild-type	Fold-Change in VIR-7832 IC_{50} vs. Wild-type
South Africa (B.1.351; Beta)	L18F, D80A, D215G, R246I, K417N, E484K, N501Y, D614G, A701V	0.6	0.7
UK (B.1.1.7; Alpha)	H69-, V70-, Y144-, N501Y, A570D, D614G, P681H, T716I, S982A, D1118H	2.3	2.5
Brazil (P.1; Gamma)	D138Y, D614G, E484K, H655Y, K417T, L18F, N501Y, P26S, R190S, T1027I, T20N, V1176F	0.4	0.4
Mexico/Swiss (B.1.1.519)	T478K, D614G, P681H, T732A	0.8	NT
New York (B.1.526; Iota)	L5F, T95I, D253G, E484K, D614G, A701V	0.6	NT
Scotland (B.1.258)	H69-, V70-, N439K, D614G,	0.9	NT
Nigeria (B.1.525; Eta)	Q52R, A67V, H69-, V70-, Y144-, E484K, D614G, Q677H, F888L	0.9	NT
US (R.2)	E484K, D614G, Q677H, T732S, E1202Q	0.8	NT
California (B.1.427/B.1.429; Epsilon)	S13I, W152C, L452R, D614G	0.7	NT
Liverpool (A.23.1)	R102I, F157L, V367F, E484K, Q613H, P681R	1.1	NT
India (B.1.617.1; Kappa)	T95I, G142D, E154K, L452R, E484Q, D614G, P681R, Q1071H	0.7	NT
India (B.1.617.2; Delta)	T19R, G142D, E156G, F157-, R158-, L452R, T478K, D614G, P681R, D950N	1.0	NT
Cameroon (B.1.619)	I210T, N440K, E484K, D614G, D936N, S939F, T1027I	1.3	NT
Bristol (B.1.1.7+E484K)	H69-, V70-, Y144-, E484K, N501Y, A570D, D614G, P681H, T716I, S982A, D1118H	1.7	NT

Table 3

Amino Acid position	Substitution / Deletion	mAb with Reduced Susceptibility	Variants in Tested Spike Sequence	VIR-7831 EC_{50} (ng/ml)	Average Fold Change in EC_{50} Compared to Relative Wild-Type
E406	W	casirivimab imdevimab		523.66	0.74
K417	E	casirivimab	K417E	67.71	0.89
N439	K	imdevimab	N439K, D614G	17.05	0.86
N440	D	imdevimab	N440D	80.47	1.29
N440	K	imdevimab	N440K, D614G	19.99	0.48
K444	Q	imdevimab	K444Q	79.68	1.11
V445	A	imdevimab	V445A	41.74	3.38
G446	V/I	imdevimab	G446V, D614G	18.41	1.50
Y453	F	casirivimab	G261D, Y453F	27.28	2.19
L455	F	casirivimab	L455F, D614G	21.65	0.56
G476	S	casirivimab	G476S	36.97	2.94
E484	K	bamlanivimab	E484K, D614G	12.91	0.33
F486	V/I	casirivimab	F486V	82.24	1.10
Y489	H	casirivimab	Y489H	92.29	1.48
F490	S	bamlanivimab	F490S	33.10	0.85
Q493	K	casirivimab, bamlanivimab	Q483K	69.79	0.98
S494	P	casirivimab, bamlanivimab	S494P, D614G	29.10	2.50

Table 4

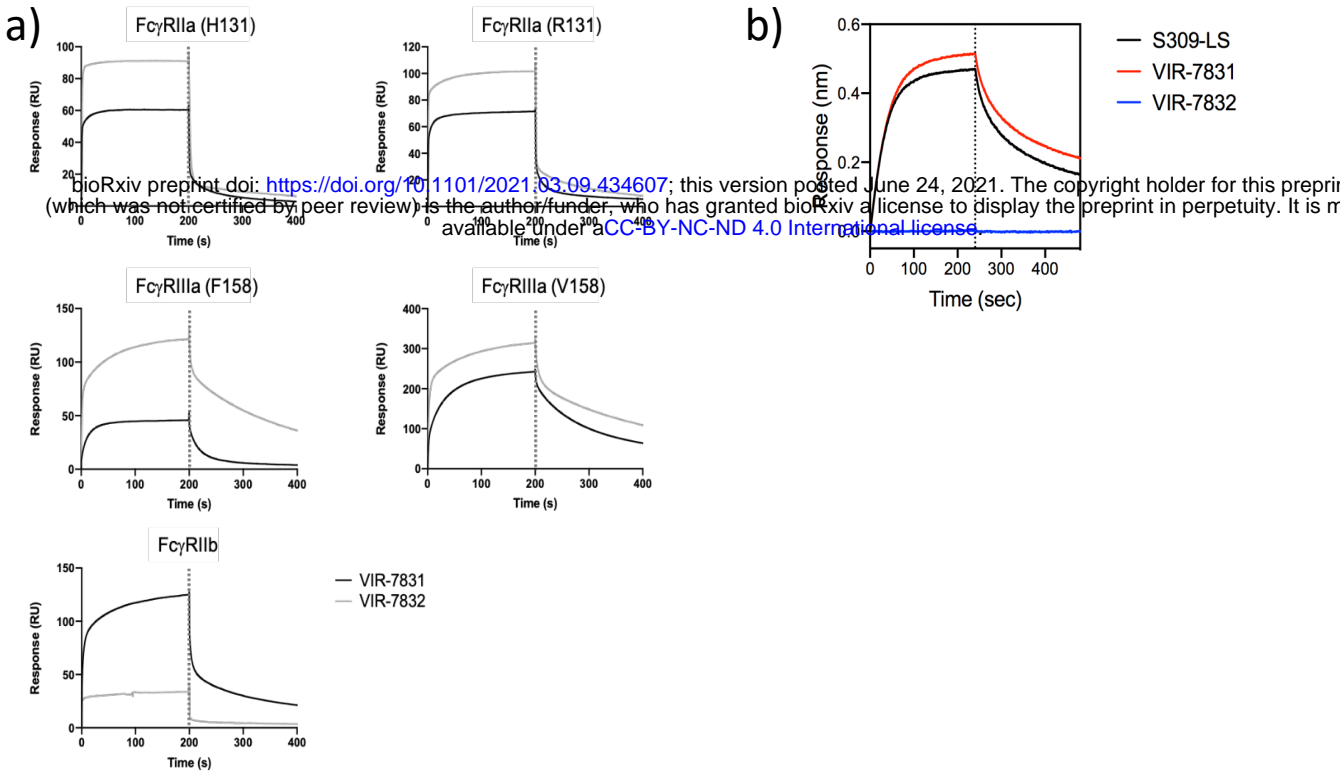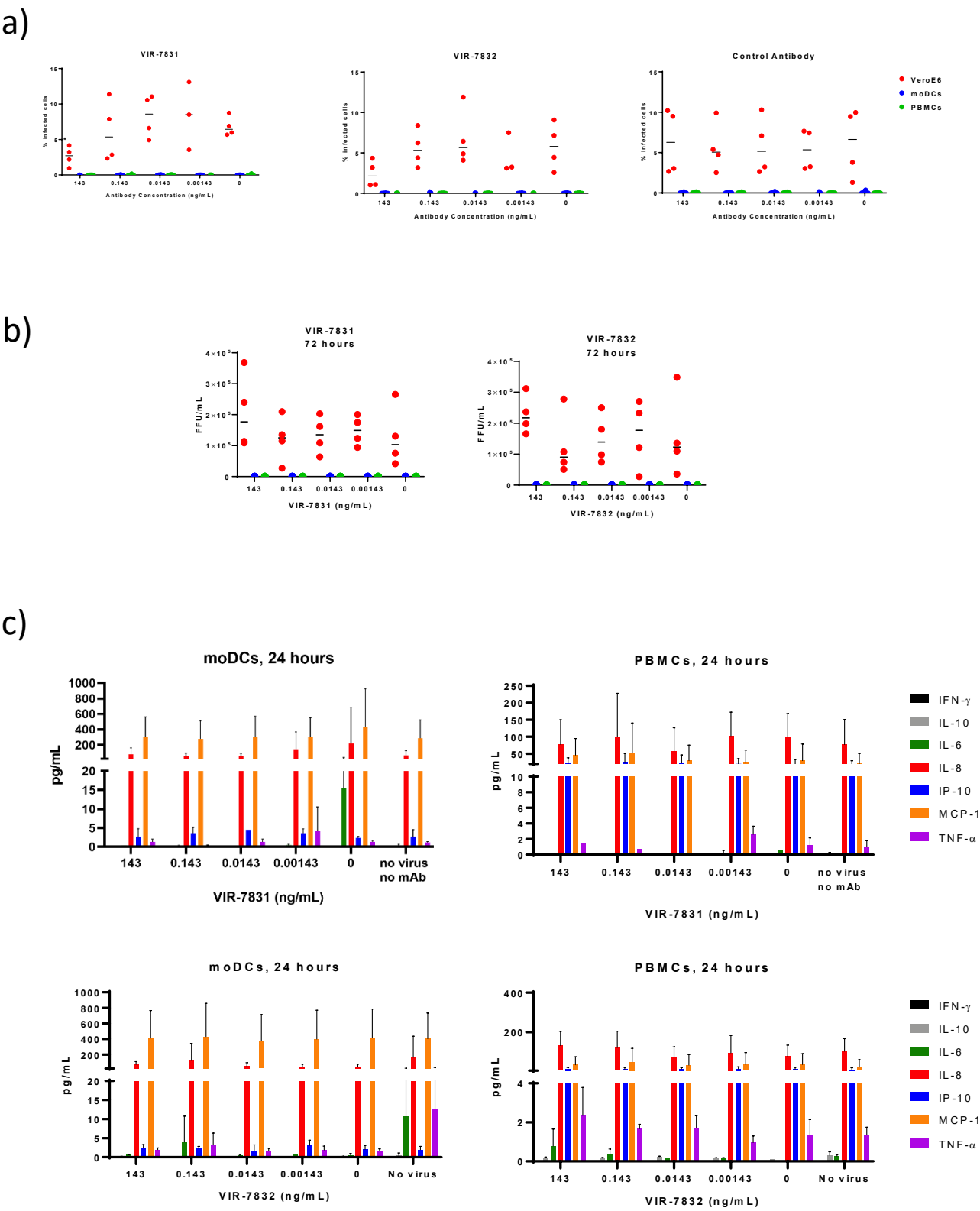| Amino Acid Position	Reference Amino Acid[a]	Variants Identified in order of Prevalence[b]	Percent Reference AA Conservation
332	I	V, T	>99.99
333	I		>99.99
334	N	**K,** H, Y, D	>99.99
335	L	**F**, S, M	99.99
336	C	S	>99.99
337	P	**S, T, L, H, R**	>99.99
339	G	**D, S**, V, **C**, F	99.98
340	E	D, **K, G, A,** Q	99.99
341	V	**I**, A, P, S	99.99
343	N	S	>99.99
344	A	**S**, V, **T**, D, F, P	99.98
345	T	**S,** I, N	>99.99
346	R	**K, I, S,** G, **T,** F	99.94
354	N	**D, K, S**, **H**, G, Y	99.96
356	K	**R,** M, **N,** T, E, Y, G	99.99
357	R	**K, I** , G	99.95
358	I	**V**, T, **L**, A, E, F	>99.99
359	S	**N**, T, **R, G**, I	99.99
360	N	S, A, T, Y	>99.99
361	C	T	>99.99
440	N	**K**, T, **Y, S, D**, I, H	99.89
441	L	**F, I**, R, V	>99.99
509	R	I, K, S, T, P	>99.99

Table 5

Epitope Reference Amino Acid	Amino Acid Changes in Spike protein	Geomean Neutralization EC$_{50}$ (ng/mL)	Average Fold-Change VIR-7831 EC$_{50}$ Relative to Wild-Type
R333	T333I, D614G	30.93	0.59
N334	N334K, D614G	45.30	1.27
L335	L335F	29.19	0.81
P337	P337H, D614G[a]	225.49	7.50
	P337L, D614G[a]	5241.44	180.46
	P337R, D614G[a]	>10000	>276
	P337S, D614G	127.69	1.26
	P337T, D614G[a]	199.78	5.38
G339	G339D, D614G	117.38	1.18
	G339S, D614G	32.67	0.63
	G339C, D614G	68.79	1.18
E340	E340A	>10000	>100
	E340K	>10000	>297
	E340G, D614G[a]	1013.97	27.47
V341	V341I, D614G	14.6	0.16
A344	A344S	92.19	0.89
	A344T, D614G	40.94	0.62
R346	R346K, D614G	24.76	0.72
	R346I, D614G	65.39	1.25
	R346S, D614G	42.87	0.82
	R346T, D614G	89.04	1.25
N354	N354D	104.8	1.00
	N354K, T95I	70.62	0.76
	N354S, D614G	61.78	0.89
	N354H, D614G	74.88	1.06
K356	K356R, D614G	29.61	0.57
	K356N, D614G	53.22	1.12
R357	R357K, D614G	39.13	0.75
	R357I, D614G	46.41	0.98
I358	I358V, D614G	32.71	0.70
	I358L	44.01	0.80
S359	S359N	95.55	0.96
	S359G, D614G	37.56	0.80
	S359R, D614G	62.0	0.89
N440	N440K, D614G	19.99	0.48
	N440Y, D614G	42.65	0.68
	N440S, D614G	51.34	0.73
L441	L441F, D614G	25.21	0.40
	L441I, D614G	32.96	0.70

Supplemental Figure 1

a)

FcγRIIa (H131)

Response (RU) vs Time (s)

FcγRIIa (R131)

Response (RU) vs Time (s)

b)

Response (nm) vs Time (sec)

— S309-LS
— VIR-7831
— VIR-7832

FcγRIIIa (F158)

Response (RU) vs Time (s)

FcγRIIIa (V158)

Response (RU) vs Time (s)

FcγRIIb

Response (RU) vs Time (s)

— VIR-7831
— VIR-7832

Supplemental Figure 2

a)

b)

c)

Supplemental Figure 3

a)

b)

c)

Supplemental Table 1

Passage	Spike Gene Amino Acid Substitution (Freq) [a],[b]	EC_{50} (µg/mL)	Fold Change in EC_{50} to WT[c]
SARS-CoV-2 virus stock[c]	H66R (5.7%)	0.06	NA
	T76I (5.6%)		
	215-216insKLRS (60.9%)		
	H655Y (3.1%)		
VIR-7832 Lineage 1, passage 4	215-216insKLRS (74.5%)	0.34	5.64
	675-679 del (20.6%)		
VIR-7832 Lineage 1, passage 5	215-216insKLRS (74.6%)	0.35	5.93
	675-679del (66.0%)		
VIR-7832 Lineage 1, passage 8	215-216insKLRS (74.7%)	ND	>10
	E340A (98.7%)		
	675-679del (84.5%)		
VIR-7832 Lineage 2, passage 5	215-216insKLRS (73.9%)	0.32	5.40
	675-679del (47.3%)		
	R682W (4.9%)		
	V1128F (3.5%)		
VIR-7832 Lineage 2, passage 6	215-216insKLRS (75.3%)	0.39	6.54
	675-679del (74.2%)		
	R682W (4.9%)		
	V1128F (30.9%)		

Supplemental Table 2

Amino Acid Changes in Spike protein	VIR-7831		VIR-7832	
	Geomean Neutralization EC_{50} (ng/mL)	Fold Change Relative to Wild-Type	Geomean Neutralization EC_{50} (ng/mL)	Fold Change Relative to Wild-Type
Wild Type	104.46	NA	100.75	NA
E340A	> 10,000	> 100	> 10,000	> 107
R682W	53.96	0.52	47.78	0.49
V1128F	50.65	0.53	49.69	0.60